Università Politecnica delle Marche
Scuola di Dottorato di Ricerca in Scienze dell'Ingegneria
Corso di Dottorato in Ingegneria Industriale

Misure Subacquee Senza Contatto per la Riproduzione della Forma e del Colore dei Coralli

Ph.D. Dissertation of:

Rachele Napolitano

Supervisor:

Prof. Enrico Primo Tomasini

Assistant Supervisor:

Dr. Paolo Chiariotti

Ph.D. Course coordinator:

Prof. F. Mandorli

XVII^{0} edition - new series

Università Politecnica delle Marche
Scuola di Dottorato di Ricerca in Scienze dell'Ingegneria
Corso di Dottorato in Ingegneria Industriale

Underwater Non-Contact Measurements for Corals Colour and Shape Assessment

Ph.D. Dissertation of:

Rachele Napolitano

Supervisor:

Prof. Enrico Primo Tomasini

Assistant Supervisor:

Dr. Paolo Chiariotti

Ph.D. Course coordinator:

Prof. F. Mandorli

XVII^0 edition - new series

Università Politecnica delle Marche
Dipartimento di Ingegneria Industriale e Scienze Matematiche (DIISM)
Via Brecce Bianche — 60131 - Ancona, Italy

Abstract

The proposal of this doctoral thesis is to understand the exploitability of scanning technologies for studying and observing the shape variability of marine sessile benthic organisms with particular focus on isolated corals in shallow water. This study aims to compare two different systems, laser-based and image-based techniques, for 3D shape reconstruction and colour information.

The first part of this thesis concerns a general description of the zonation, morphology and biological monitoring of the coral reef, in order to collocate this work in a larger project, in which the possibility to describe the modification of the bottom topography by means of underwater 3D sensors is an important contribution for the marine flora and fauna. A brief review of the underwater scanning methods is performed, highlighting the advantages and the drawbacks of the different solutions.

The approach to the study is schematized by describing the different case studies (terrestrial and underwater conditions) adopted for the survey of small-sized samples, supported by laboratory tests. A particular focus is on the reduction of the underwater images quality in the photogrammetric approach, limited by the light attenuation. This is a fundamental issue, mainly for the acquisition in shallow water where the artificial light may not be an exploitable solution. For this reason, the investigation involves the implementation of a colour correction algorithm to restore the degraded images. The main contribution of this image pre-processing step is the drastically improvement of the matching point recognition and the reconstruction of the whole object independently to environmental illumination changes.

The results show the difference between the 3D models obtained from a prototype 3D colour laser scanner (RGB-ITR) developed in ENEA ArtVisLab (Frascati) and a photogrammetric approach based on standard commercial cameras with different optical lenses.

The colour and shape reconstruction capabilities of the latter technique, which proved to be superior to the laser-based one in underwater applications, were metrologically assessed by dedicated tests.

Contents

1. Introduction 1

2. State of the art 4

2.1. Coral Reefs Populations 4
2.1.1. Spatial Distribution and Zonation 5
2.1.1.1. Corals Shape and Morphological Descriptors 7
2.1.2. Determination of Growth Rates 9
2.2. Underwater Scanning Methods and Optical Sensors 11
2.2.1. Time of Flight 12
2.2.1.1. Sonar 12
2.2.1.2. LiDAR 13
2.2.1.3. Pulse Gated LLS 13
2.2.2. Modulation 14
2.2.2.1. Modulated LLS 14
2.2.3. Triangulation 14
2.2.3.1. Continuous Wave LLS 14
2.2.3.2. Structured light 15
2.2.3.3. Stereo vision 16
2.2.3.4. Underwater Photogrammetry 17

3. Testing of the Laser-Based Method for Underwater Application 19

3.1. Acquisition System: RGB-ITR Laser Scanner 19
3.2. Acquisition Procedure 21
3.2.1. Case study: Terrestrial Application 21
3.2.2. Case study: Underwater Application 22
3.3. Image Processing and 3D Reconstruction 23

4. Implementation of a Colour-Correction Algorithm for Underwater Photogrammetry 24

4.1. Image Processing Issues in Underwater Application 24
4.2. Proposed Method for the Colour Correction 26
4.2.1. Contrast Enhancement Technique: CLAHE Algorithm 27
4.2.2. Colour Balance Adjustment 27
4.2.3. Gamma Correction Algorithm 28

5. Evaluation of the Photogrammetric Method for Underwater Application.....29

5.1. Acquisition System: Camera for Detailed Scanning 29
5.2. Acquisition Procedure 31
5.2.1. Case study: Terrestrial Application 32
5.2.2. Case study: Underwater Application 32
5.2.2.1. Dataset: Target immersed in water 33
5.2.2.2. Dataset: Target and Camera immersed in water 34
5.3. 3D Reconstruction and Modelling 36
5.4. Geo-Referencing and Scaling Procedures 36

6. Results and Discussion 37

6.1. RGB-ITR Laser Scanner Results 37
6.1.1. Case study: Terrestrial Application 37
6.1.2. Case study: Underwater Application 40
6.2. Colour Correction Algorithm Results 42
6.2.1. Contrast Enhancement Results 42
6.2.2. Colour Balance Adjustment Results 42
6.2.3. Gamma Correction Algorithm Results 43
6.3. Photogrammetric Results 46
6.3.1. Case study: Terrestrial Application 46
6.3.2. Case study: Underwater Application 47
6.3.2.1. Dataset: Target immersed in water 48
6.3.2.2. Dataset: Target and Camera immersed in water 49

7. Quantitative Assessment for Photogrammetric Colour and Shape Reconstruction 52

7.1. Colour Validation 52
7.1.1. Spectrophotometer as Gold Standard 53
7.1.2. Image Colour Correction Accuracy 54
7.2. 3D Shape Validation 56
7.2.1. Laser Displacement Sensor as Gold Standard 56
7.2.2. 3D Reconstruction Accuracy 57

8. Conclusions 61

References 64

List of Figures

Figure 1 Geological evolution of coral reefs, from fringing reef (left), to the barrier reefs (centre) and finally to the atolls (right) [12]. 6
Figure 2 The basic morphological categories according to the environmental stresses [16]. 7
Figure 3 Distribution of the different coral shapes across the different reef sections [16]. ... 8
Figure 4 a) Marking of colonies with vital dye. b) Bryozoan Pentapora facialis laminates marked with red Alizarin [14]. 10
Figure 5 Underwater 3D reconstruction classification [27]. 11
Figure 6 Pulse Ranging [41]. 13
Figure 7 A scheme of a structured light scanning [61]. 16
Figure 8 Triangulation geometry principle for a stereo system [63]. 16
Figure 9 Light absorption in underwater environment that grows gradually with depth. 17
Figure 10 An example of calibrated reflectance values of the three channels: up there is the back-reflected signal of a grey target at different distances, below the back-reflected signal of a black one. 20
Figure 11 From right to left: the three adopted samples with growing complexity structure. 21
Figure 12 The CR immersed in the aquarium and the PC in a matt bucket. 22
Figure 13 Configuration of the underwater acquisition with the RGB-ITR 22
Figure 14 User interface of ScanSystem (a) and ITR Analyzer (b) software modules. 23
Figure 15 Transmittance for the three wavelengths corresponding to the RGB colour channels. 25
Figure 16 Block diagram of the proposed method. 26
Figure 17 Varying gamma values 28
Figure 18 Difference between the refraction due to a flat port (a) and a dome port interface (b) and the underwater housing used in the test laboraotry. 30
Figure 19 An example of photos of the PV acquired in-air condition and with different lighting illumination. 32
Figure 20 Set up of the described dataset 33
Figure 21 An example of images acquired with sample immersed in the aquarium. 33
Figure 22 Data acquisition with sample and camera immersed in water. 34
Figure 23 An example of sample acquired in water. 34
Figure 24 An example of colour profile on a row of the normalized image. 37

Figure 25 An example of the manually selection of the reference points between the two meshes (a) and the correspondent distance errors (b). 38
Figure 26 Screen of different configurations of the CR (a), CP (b) and the IC (c) acquired in-air condition. 39
Figure 27 The z-profile of a row of the CR (a), the PC (b) and the IC (c). 39
Figure 28 Screen of different configurations of the CR (a) and the PC (b) acquired in water. 40
Figure 29 The z-profile of one row of the CR (a) and the PC (b) in water condition. 41
Figure 30 Example of colour enhancement result: on the left there is the original image histogram, on the right there is the stretched colour image histogram. 42
Figure 31 Example of colour balanced result: on the left there is the histogram of the contrast enhanced image, on the right there is the image histogram with grey balance applied. 43
Figure 32 Visualization of the estimated illuminant and the ground trouth of two images with different lighting conditions. Each illuminant represents a vector in RGB space. 43
Figure 33 Comparison between the histogram obtained after the colour balancing (on the left) and the histogram of the final colour corrected image (on the right). 44
Figure 34 Comparison between the colours corrected histogram of two consecutive images acquired with different lighting conditions. 44
Figure 35 Result of the colour restoration of two images with different lighting conditions: on the left there are the original images, in the centre there are the enhanced images and on the right there are the final corrected colour images. 45
Figure 36 Result of the colour restoration of two underwater images: on the left there are the original images, in the centre there are the enhanced images and on the right there are the final corrected colour image. 45
Figure 37 3D models acquired in-air condition by means of the 16 mm lens (a), the 60 mm lens (b) and the 18-105 mm lens(c). 47
Figure 38 3D models obtained from dataset 2 by means of the 16 mm lens (a), the 60 mm lens (b) and the 18-105 mm lens(c). 48
Figure 39 3D models obtained from dataset 2 by means of the 16 mm lens (a), the 60 mm lens (b) and the 18-105 mm lens(c). 49
Figure 40 Estimated distances on the 3D models obtained by means of the 16mm lens. 50
Figure 41 Estimated distances on the 3D models obtained by means of the 60mm lens. 50
Figure 42 Estimated distances on the 3D models obtained by means of the zoom lens. 51
Figure 43 The 9 reference tiles used for the colour validation procedure and the whit target (D65 illuminant) in the centre. 53

Figure 44 MCDM and standard deviation of images acquired in-air condition. 55
Figure 45 Mean and standard deviation of colour difference of underwater images. 56
Figure 46 Sample specifications (on the left) and the set up measurement for determination of reference points (on the right). 57
Figure 47 Comparison of the points measured on the z-profiles of the models obtained with different camera lenses in-air condition and the reference points. 58
Figure 48 Correlation between the reference and estimated data. 59
Figure 49 Comparison of the points measured on the z-profiles of the models obtained with different camera lenses in water condition and the reference points. 60
Figure 50 Correlation between the reference and estimated data in water condition. 60
Figure 51 Block diagram of a digital cameras for the formation of the digital image [109]. 66
Figure 52 Photogrammetric 3D reconstruction procedure schematized 69
Figure 53 Comparison between the alignment phase of the original (a) and the corrected images (b) 70

List of Tables

Table 1 Some main characteristic of the different scanning methods. 18
Table 2 Cameras features 29
Table 3 Acquisition parameters for sample acquired in air condition. 35
Table 4 Acquisition parameters for sample immersed in the aquarium. 35
Table 5 Acquisition parameters for sample and cameras immersed in the water tank. 35
Table 6 3D data models summarized. 46
Table 7 Total error calculated on the eight reference points for dataset 1. 47
Table 8 Total error calculated on the eight reference points for dataset 2. 48
Table 9 Total error calculated on the eight reference points for dataset 3. 49
Table 10 Colour difference measured by spectrophotometer for 9 tiles 53
Table 11 Summarized results for each tile in images acquired in-air. 54
Table 12 Summarized results for each tile in underwater images 55
Table 13 Measurements results of the laser displacement sensor 57
Table 14 Summary results obtained for the sample acquired in-air condition. 58
Table 15 Summary results obtained for the sample acquired in water condition. 59
Table 16 Classification of lens focal lengths, types and general uses. 67

1. Introduction

The idea underlying this research, carried out at the Polytechnic University of Marche and in collaboration with the Anton Dorhn Zoological Station (Naples), is to transfer the technology of laser-based and image-based 3D shape measurements, which have been proved to provide outstanding performances in terms of accuracy and resolution in standard outside-water applications, to the "underwater world".

The applications of these technologies to the underwater environment range from the cultural heritage to engineering, to the marine biology and marine geology fields. And exactly in this latter area, the development of this activity is placed.

For what concern 3D shape measurement in underwater applications, it has always represented a challenging task. The necessity to work in an environment characterized by different light conditions and particulate concentrations, the need of having high-performance sealing and, last but not least, portability of devices involved in the measurement process have limited the range of possible measurement techniques among those available for 3D shape reconstruction. Indeed, portability also represents a challenge, especially when measurement devices should be carried by scuba divers.

When thinking to marine biology applications it should be clear that the possibility to describe the reef typology and to study populations and assemblages of sessile habitat-former organisms (mainly anthozoans) by means of non-contact measurements is essential to preserve and protect this highly valuable habitat-former species and the systems they have built.

Within this contest, the possibility to perform accurate measurements of volume, surface area and other morphometric measurements, plays an important role for correctly classifying marine organisms and their biodiversity. Indeed, this is tightly linked with studies on biological evolution and marine ecosystem dynamics, using an integrated and interdisciplinary approach, that range.

The analysis of the coral reef can be carried out by means of a multiscale approach: from the observation of large areas of the seabed, to the details of small structures concentrated on small areas. Therefore, it is necessary to consider different levels of detail, ranging from the meter, to the centimetre, up to the millimetre. All these aspects have necessarily implied a trade-off between accuracy and applicability of certain measurement techniques.

The aim of this doctoral thesis is to explore different non-contact methods, namely a laser-based solution and an imaging approach, for underwater measurements. For this purpose, a prototype of terrestrial laser scanner, with three different wavelengths (at 650 nm, 532 nm, 450 nm) and the underwater photogrammetry were tested.

It is well accepted that, nowadays, measurement technologies applied to the underwater environment are typically, and successfully, used for large scale (macro-scale) scanning of coral reefs. On the contrary, this research activity focuses on the micro-scale, i.e. for the scanning of individual corals on a superficial reef flat. So, the approach to the underwater world and in particular to the benthic organisms in shallow water, has led to meet challenges

in the optics field, imposing various measures due to the various typical issues in this environment.

In particular, the basic requirements that the tested technologies had to satisfy are mainly three:

- Capability of working in non-uniform lighting conditions and with external objects that could interfere with the scene framed (e.g. external objects projecting shadows or obscuring the target).
- Capability of investigating different sizes and characteristic of the submersed object.
- Fast and easy-to-do processing of data acquired in-situ.

For this reason, in addition to the metric accuracy of the examined objects, in this context the colorimetric information plays an important role. This aspect plays a secondary role in typical underwater applications. It will be shown that a pre-processing step, in which the compensation of underwater images is performed to restore the scene actual colours and contrast in non-uniform lighting conditions, provides benefits both in terms of coral colour extraction capabilities and accuracy in the 3D shape reconstruction.

The research activity is structured with four main goals:

Goal 1. *Identification of main issues in adapting already existing solutions to underwater applications*

During this step, carried out in the first year, a comprehensive and detailed analysis of criticalities of up-to-date devices used in outside-water application was performed. This task is served as a grounding basis for steering the following research activity.

Goal 2. *Comparison of laboratory-scale instruments using experimental analyses*

The identification of the measurement principles, acquisition and data processing strategies are the main objective of this research stage.

The two scanning systems (the laser scanner and the photogrammetric cameras) were identified and compared, and simulations supported by lab-scale experimental tests were performed to pinpoint the effectiveness and weakness of the solutions identified during transfer to underwater environment.

The following aspects were analysed:

- Definition of proper data acquisition and processing strategies;
- Colour correction and illumination of the shooting scene.

Different measuring conditions were also simulated and tested:

- Different lighting conditions;
- Different sizes and characteristics of target object.

Goal 3. *Implementation of a colour correction algorithm to enhance the 3D reconstruction*

During this step a method for improving the photogrammetric image processing was implemented to produce more uniform and detailed images by correcting the different lighting conditions influence, which can spoil the 3D reconstruction. Also for the laser-based method, a colour calibration procedure is applied in order to balance the colour of acquired scene and it is an integrated part of the user interface software.

Goal 4. *Results analysis and measurement uncertainties*

During this phase, the results and the 3D models were analysed and compared. Furthermore, the measurement uncertainties relating to the colour obtained with the implemented image correction algorithm and those relating to the 3D shape obtained from the reconstructions outside and in the water was determined.

This thesis begins with a literature review in Chapter 2, introducing the submarine world and the 3D data capture and modelling technologies used in this environment. This Chapter is composed by two main parts. In the first one, the marine benthos distribution and the traditional methods for morphological description are described. Section 2.2 describes the classification of the underwater scanning methods based on the measuring principles and reviews the used technologies.

Chapter 3 describes the laser-based method used in the first part of the laboratory tests, details the data acquisition and explains the processing methodology for the 3D reconstruction.

Chapter 4 gives a detailed explanation of an implemented algorithm to restore colours and illumination of an underwater scene. This chapter is tightly related to the next chapter, because concerns the pre-processing phase of the sets of images acquired by means of the photogrammetric approach.

Chapter 5 discusses the application of the image-based method for the underwater survey and highlights the experimental section characterized by the assessment of the device for a detailed scanning of small targets. In Appendix A, the general concepts of digital photography are described in details and in Appendix B there is highlight the difference between the reconstruction procedure of original and corrected images

In Chapter 6, the colour correction algorithm and the 3D models obtained by photogrammetry are proved to be effective by comparing results on simplified models tested with two reference measurement techniques, respectively Spectrophotometry for colour extraction and Laser Displacement Sensor for the target dimensional assessment. Therefore, the uncertainty analysis associated to the colour and dimensional measurements is discussed.

The thesis concludes with a brief summary, discussion and possible future work in Chapter 7.

In order to provide the general concepts on camera sensors, digital image and camera lenses classification, the Appendix A is dedicated, while Appendix B provides a detailed description of the reconstruction software used in the trial.

2. State of the art

This chapter refers to the general description of the underwater ecosystem characterized by reef-building corals and the differences between the biological and optical systems adopted for the underwater survey. First, a description of coral reef in terms of ecology, distribution and morphological descriptors is carried out. This is essential to understand the placement and impact of this work. The available biological monitoring methods to detect marine populations and communities are also described.

Then, a review of non-contact scanning methods for monitoring the marine environment is conducted. The main strengths and weaknesses of solutions available to researchers are summarized in this chapter.

2.1 Coral Reefs Populations

Coral reefs are some of the most iconic seascapes in the world and are also characterized by the wide and diversified species ranging from planktonic organisms that represent the base of the marine food web to large marine mammal [1]. Reef-building corals provide homes to fish and invertebrates and support other coastal ecosystems by protecting the shoreline.

Usually, this organisms have a complex morphology and 3D structure and they represent habitat formers for other associated plant and animals (engineering species) [2]. In hard bottoms, habitat forming species are not restricted to corals (athozoans and gorgonaceans), but, are represented by other sessile colonial invertebrates, as for example sponges and bryozoans, as well as by some plant species, as conspicuous brown algae (Fucales) and red Corallinales algae. One of the main ecological role of these habitat formers is to modify the bottom topography and to increase the architectural complexity and the biodiversity at different scales. In addition, many of such engineering, including bio-constructor species, especially among scleractinian corals, sponges and bryozoans, are quite plastic in their morphology and have the capacity to change their shape according to local environmental condition [3]. While in some case, they also represent species sensitive to climate changes and therefore bioindicator of water warming, and can register past climatic events in their skeletons [4, 5]. The increase in human activities, e.g. over-exploitation, pollution, etc. increase the risk to damage the marine ecosystem. [6]. In particular, in the recent years the coral populations are affected by global warming and ocean acidification, leading to an increase in its mortality rate [7]. For this reason it is very important the safeguard of the marine ecosystem.

Due to the high vulnerability of these bio-constructor organisms, action plans for their conservation should be a priority. The increase of knowledge is essential for the conservation and protection of this highly valuable habitat-former species and the systems they built. For these reasons, there is the need to provide a description of the reef typology and, in general, to study populations and assemblages of sessile habitat-former organisms.

The focus of biological monitoring is precisely to provide how they modify the bottom topography and the ecological implications. The main state variables of interest include the abundance, the population density, the biomass, the population structure, the biodiversity, and the occupancy.

However, biodiversity is the hardest topic to monitor and assess because so many species are tiny, rare, and hidden in the framework of the reef. Moreover, it is necessary to take into account different levels of accuracy, considering three different types of structures:

1. **Community structure**, carried out with a detail level less than 1 meter, in which the measurement system is required to operate at great distances (10-100 m) even in turbid waters. The purpose of this analysis is the patrolling of difficult environments, such as backdrops or caves, in which it is not possible to access through Remote Operated Vehicles (ROV's). In this way, it is possible to evaluate the overall conformation and the macro-porosity.
2. **Population structure**, carried out with a detail level around the centimetre, in which the system can operate even at shorter distances (1-10 m). The performance in turbid waters is lower compared to that of rapidity of measurement and accuracy in operating conditions. The aim of this analysis is the evaluation of the superficial porosity and the steric configuration of the habitat, in order to establish the diversity of the analysed population.
3. **Colonies and individuals**, in which the accuracy and resolution of the measurement must be extremely high, with a detail level less than 1 millimetre. This analysis, combined with 3D Additive Manufacturing, can provide accurate and fast representation of small colonies.

2.1.1 Spatial Distribution and Zonation

Before describing the morphological characteristics of the marine populations, it is necessary to distinguish three different kinds of coral reef formations: the fringing reef, barrier reef and atoll (Figure 1). Darwin believed that these formations are a consequence of a long-term reef growth process [8].

The most common type is the first one, also called marginal or areal reef (over 50% of the world's coral reefs are fringing type, in particular in the Caribbean and Red Seas) [9]. This kind of reef grows in direct contact with the coast, forming borders along the shoreline and surrounding islands.

Instead, barrier reefs are separated by the shore from a lagoon of deep water but are very similar to the fringing reef.

Another type of coral reef is that formed by the coral atolls, constituted by the progressive disappearance of a volcanic island which, while leaving the fringed barriers surrounding it in remote ages intact, has then generated an inner lagoon, surrounded by a coral ring more or less regular (e.g.: Maldivian and Polynesian atolls).

The current reefs formations are mainly developed between the surface and the 30 meters depth, but only in waters with a year temperature never lower than 21° C.

Other factors that limit the coral reefs growth and diffusion are the water salinity which must be constant, the intense radiation of the environment in which they live (necessary for the photosynthesis process of the zooxanthellae algae hosted in the coral tissues) and finally, the sedimentation rate [10].

Their distribution varied considerably over time: phases of great geographical expansion alternated with others of contraction, due to the continuous climatic changes [11].

Currently, this delicate ecosystem is once again in danger and risks disappearing, for countless reasons. The main cause of reef rarefaction seems to be linked to climate change (warming and ocean acidification), pollution and corals bleaching.
The corals bleaching is a phenomenon that consists in the expulsion of zooxanthella algae, which normally live in symbiosis in the tissues of the corals themselves. Without them the coral results to be more fragile and thus bringing it to death. This is a consequence of a strong stress likely due to an excessive warming of the surrounding waters that is nowadays triggered by global climate changes. The combined action of local anthropic activity (such as overfishing and declining water quality) also increases the environmental stress on coral ecosystems.

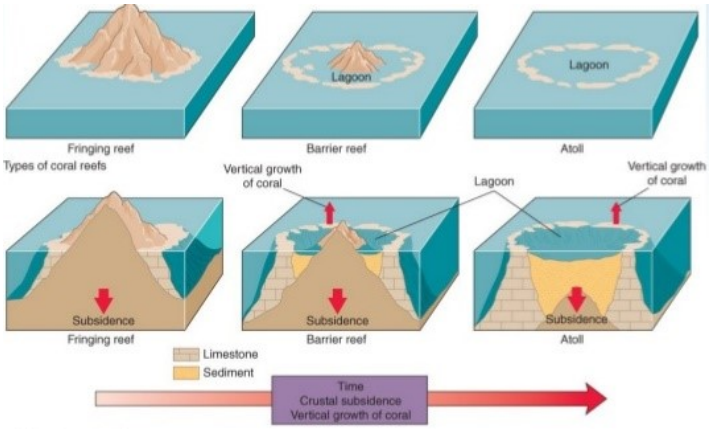

Figure 1 Geological evolution of coral reefs, from fringing reef (left), to the barrier reefs (centre) and finally to the atolls (right) [12].

It is possible to describe a regular succession of species (zonation model) of the coral reefs influenced by all the factors that affect the overall development, so the light exposure, the wave stress, the sediment flux and the subaerial exposure [13], characterizing two main zones (Figure 3):

- The *flat reef*, relatively shallow and closest to shore. In these shallow waters occur wide variations in temperature and salinity and a higher accumulation of sediments.
- The *fore reef*, farther out to sea, is often quite steep, and descends to depths too great to allow the growth of coral. Coral grows much more abundantly on the slope, both in numbers and in species diversity. This is mostly because sediments are less concentrated here. Greater wave action disperses pollutants and carries nutrients to this area.

In the following section, the shape of corals, which depends on different environmental variables, are classified. In addition, the main dimensional parameters are highlighted to describe their size.

2.1.1.1 Corals Shape and Morphological Descriptors

It is necessary to distinguish the marine benthos in two different groups of organisms: the clonal benthic organisms (modular organisms), organized to form colonies, and aclonal benthic organisms (non-modular organisms), characterized by single units [14]. In the first one, the modules are genetically identical units, unlike the second one that are genetically unique and with different individual shapes of the same species.

The modularity of clonal organisms provides great flexibility in terms of growth. The functional units of the clonal organisms can be added in various parts of the organism by directing growth in various directions, expressing thus a morphological plasticity strongly influenced by local environmental conditions.

It is common to identify categories of invertebrates whose morphology is similar also for different systematic groups. On the contrary, the different growth forms and the structural differences within the same species (aclonal organisms) cannot be obvious.

The basic morphological forms were recognized for clonal organisms as a function of the several factors listed above (Figure 2) [15].

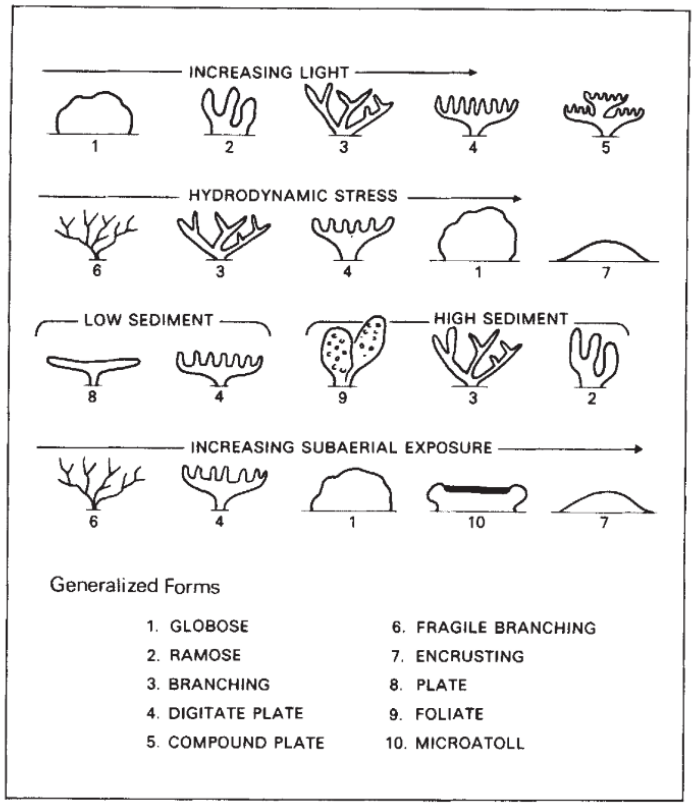

Figure 2 The basic morphological categories according to the environmental stresses [16].

The 10 morphological categories or growth strategies can be defined as follows:

1. *Globose*: typical of organisms that grow parallel, in linear or branched way, to the substrate more or less constantly.
2. *Ramose*: typical of erect, semi-erect or climbing organisms with regular or irregular ramifications and with restricted areas of attachment to the substrate.
3. *Branching*: typical of erect organisms and generally regularly branched, with a restricted area of attachment to the substrate.
4. *Digitate plate:* small, un-splitting branches which resemble fingers ('digits'). Often provide important nursery areas for juvenile reef fishes.
5. *Compound plate:* as the digitate plate shape but the colony size is extended through adding more branches.
6. *Fragile Branching*: as the typically branching shape but more thin.
7. *Encrusting:* characterized by low spreading growth forms that usually adhere to hard rocky surfaces.
8. *Plate*: typical of thin that grow more or less parallel to the substrate and are projected into the water column by limited areas of the basal attack.
9. *Foliate*: thin, plate like corals which grow in 3-D Shapes, often resembling plants (foliage). These corals tend to grow in areas with high levels of sunlight.
10. *Microatoll*: growth is mainly lateral, as upward growth is limited by exposure to air.

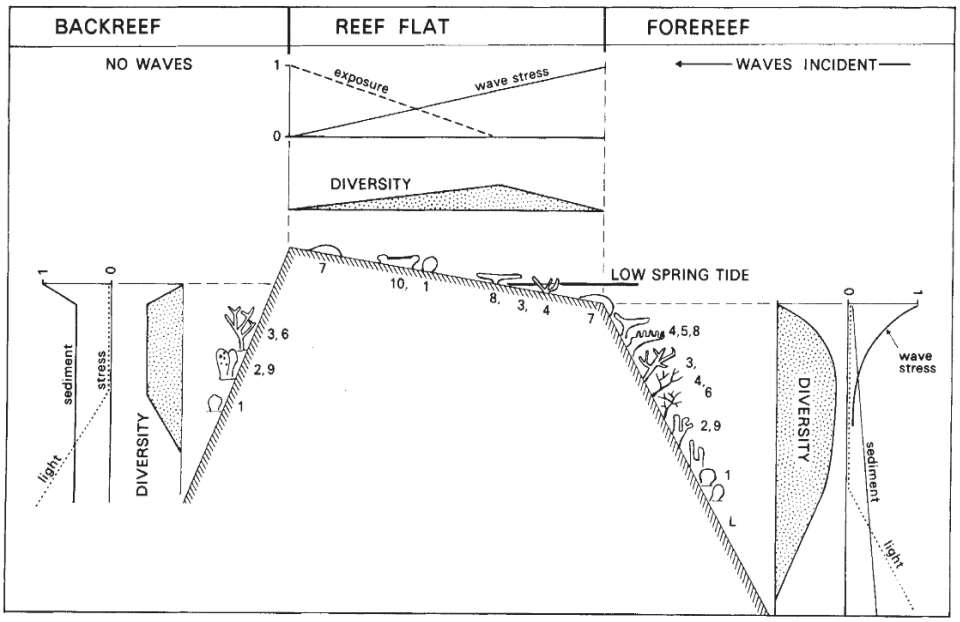

Figure 3 Distribution of the different coral shapes across the different reef sections [16].

Nine are the dimensional parameters important to define the organism size to take into consideration [14]:

1) surface tissue area (At);
2) tissues volume (Vt);
3) skeleton volume (Vsk);
4) encrusted substrate area (Se);
5) shaded substrate area (Ss);
6) perimeter of the animal portion in direct contact with the substrate (Cs);
7) maximum linear dimension reached along the substrate (Ds);
8) height on the substrate (Ht);
9) area of exposed skeleton surface or cuticular tissues (Ask).

In this way, it is possible to describe the organisms shape as the ratios between the nine size parameters. The use of morphological categories is a non-destructive method that allows gathering of information by people with limited experience in taxonomic identification. However, for some morphological categories, standardization may not always be easy and it may not sometimes be possible.

Studies relating to the growth of individuals comprising a population are based on different types of analyses and include both non-destructive and destructive methods. In the following section, a review of the applied monitoring approaches for each of the main marine components is described.

2.1.2 Determination of Growth Rates

Various methods for describing coral reefs have been developed for decades but today this is still an active research field. The focus of biological monitoring is typically to detect the occurrence and degree of change through time and space, and assess this against known impacts or management actions [17], with the aim of preserving or enhancing biodiversity, ecosystem services and natural capital assets.

Before describing the different monitoring methods, it is important to consider potential sources of error that can lead to spurious conclusions and false management actions. Estimations of state variables for populations or communities are potentially susceptible to two main sources of error: spatial variation due to the inability to survey the entire area of interest because of its large size, and imperfect detectability due to the inability to detect all individuals or even all species in surveyed areas [18].

A wide range of approaches have been developed to estimate coral growth across different time scales [19], from sub-annual up to decadal scale, and are based on different types of analyses, including both destructive and non-destructive methods [20].

The first one aims to provide the measure by removing the targets from the natural environments and performing the measure in controlled environments, such as in aquariums or in mesocosms. However, the captive conditions, even if carefully controlled, cannot never coincide with natural environment, so the measures result distorted compared to those obtained in situ. On the other hand, in the natural environment, tracing previously measured individuals may not be easy. In some case, it is necessary to delimit the study area, fixing a

square to the substrate, within which the individuals are identified and followed in exam using the photographic technique that allows to directly highlight variations in shape and size [14].

The direct growth determination in-situ is obtained by calculating some biometric parameter of a certain number of individuals in different time intervals by means of transect or using the vital dyeing method (Figure 4), for marking daily growth in scleractinian corals [21]. Carbonate skeleton bodies allow the application of a similar procedure that uses radioactive markers for the signature [22].

Labelling is another method experimented in-situ, through the insertion of nylon threads and measuring the elongation in following space and time, acquiring the scene by means of photographic detection techniques.

The indirect methods, can be mainly schematize in X-ray methods, based on the observation of regular deposition circles of limestone structures and in the analysis of population size/frequency distributions based methods. The radiographic survey is a destructive method that requires collection of samples, suitably cleaned and separated or cut into appropriate thickness units, which are subsequently subjected to radiographic survey [23].

Minor application, given the significant costs, has instead the analysis of oxygen isotopes, incorporated into the skeletal portion and measured at a regular distance from the base to the top of the colony. The analysis, carried out with mass spectrometer, allow to identify seasonal growth variations through the relationship with the water temperature [24].

For what concern methods based on the analysis of size / frequency distributions of the populations, the modal sizes are identified: each of these should approximate the length of an age class. The modal position can not often be easily identified, but if there are distributions of sizes in subsequent years, a diagram can be constructed in which the lengths are shown as function of the time and the growth rate can be estimated [14].

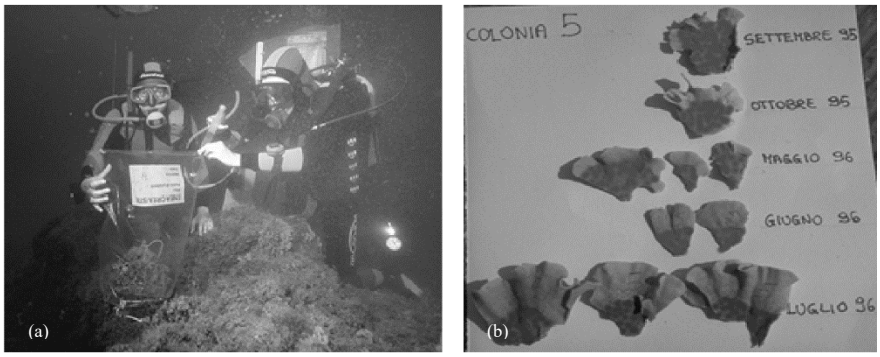

Figure 4 a) Marking of colonies with vital dye. b) Bryozoan Pentapora facialis laminates marked with red Alizarin [14].

2.2 Underwater Scanning Methods and Optical Sensors

Underwater imaging is an important tool to understand the many geological and biological processes taking place on the seabed.

There are several methods for recovering 3D information of terrestrial scene but underwater application has always represented a challenging task. Certainly, the propagation of light in the sea influences the overall performance of underwater optical systems. Indeed, water absorption and scattering phenomena have to be taken into account. In addition, scanning systems in shallow waters (<1 m) can be seriously affected by flickering, which produces strong light fluctuations due to the sunlight refraction on a waving air-water interface. Flickering generates quick changes in the appearance of the scene, making basic image processing functions, like feature extraction and matching, which are frequently used by mapping software, more difficult [25]. Last but not least, the need of having high-performance sealing and the portability have limited the range of possible measurement techniques, among those available on terrestrial environment, for 3D shape reconstruction.

Indeed, portability also represents a challenge, since devices that could be carried by scuba divers or ROV's are developed.

According to the technology and measuring principle used, underwater scanning methods can be generally classified into active and passive techniques [26].

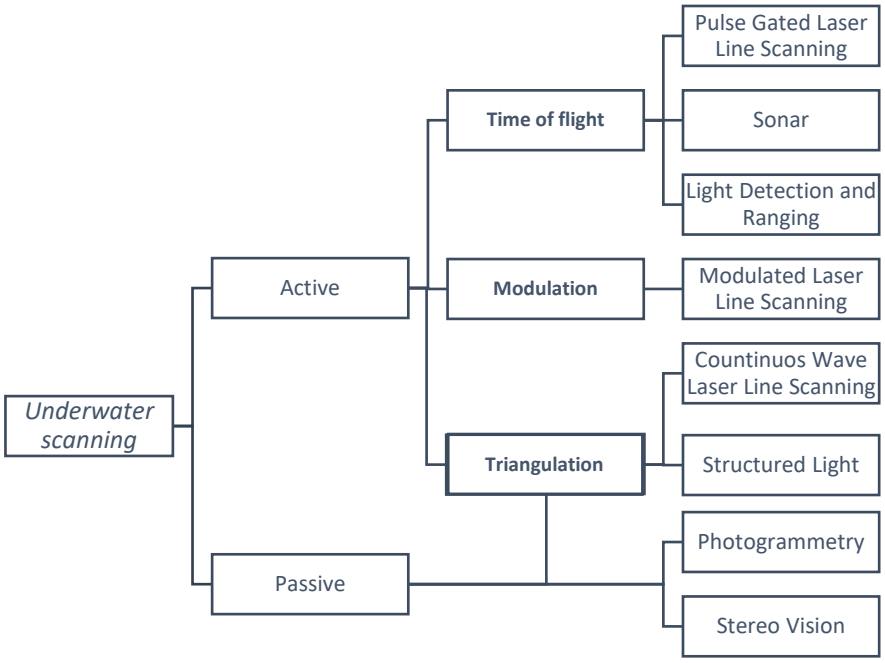

Figure 5 Underwater 3D reconstruction classification [27].

Active optical methods use radiations that act as a probe for the surface. In other words, the active sensors produce a signal to measure 3D data to be collected. On the contrary, passive optical methods use artificial light to illuminate the scene without interacting with the object and 3D shape information are obtained only by photographic images. However, it should be taken into consideration that not all these methods provide colorimetric information, structural morphology and distribution, at the same time (Figure 5).

In the following section, the technologies for the underwater scanning are classified into three main classes according to the measuring principle.

2.2.1 Time of Flight

Time discrimination methods allow to perform measurements since hundreds of meters, with a sub-centimetre precision.

The time between the emission of the signal, reflected by the object, and its return to the sensor is accurately measured. By knowing the speed of the signal in the medium where it travels, the distance can be drawn as in (1):

$$D = \frac{v*\Delta T}{2} \tag{1}$$

where: D is the distance, v is the speed of signal propagation and t is the time elapsed between the pulse emission and its reception.

These methods provides long distance measurements, especially the sonar, which is also most sensitive to the water temperature, salinity and pressure changes, altering the sound speed. At short distances, the measures are affected by small inaccuracy or great relative error. Indeed, a minimum distance measurement is required for some sensors [27].

Other main problem of these measurement systems is to determine the exact moment when the reflected signal strikes the target. In addition, the measurement precision depends on the quality of the instrument used to determine the time spent and the signal processing: the main parameters that influence the precision are the acquisition distance, the angle of incidence, and the characteristics of the surface.

Sonar, LiDAR and Pulse Gated Laser Line Scanning (PG-LLS) are some examples of sensors using this principle to acquire 3D data.

2.2.1.1 Sonar

Sonar systems are widely used in underwater measurements and are an example of active systems [28, 29]. These methods use sound propagation to perform detection and make it possible to reconstruct distances in a plane perpendicular to the ship track. Each beam gives the possibility to calculate the 3D coordinates of the point where the beam meets the seabed surface. An important advantage of this system is that sound propagation in water is faster than in air. For this reason, the sensors provide higher resolution in a range of about tenths of meters per sounding, even for thousands of meters depth. However, this is an important limitation at shorter distances: for example, at 40 m with respect to the seabed, the resolution drops to a couple of meters or less, not enough for survey small features of small structures, as the corals.

It is possible to distinguish different kinds of sonar systems:

- the Single Beam Sonar (SBS), that retrieves 3D data by rotating its head [30];
- the Side Scan Sonar (SSS) that performs a gridded survey [31];
- the Multi Beam Sonar (MBS), which performs a complete 3D scan in a stationary position [32] and can integrate a camera for colour information [33];
- the Imaging Sonar (IS) that transmits sound pulses and converts the returning echoes into digital images [34].

2.2.1.2 Light Detection and Ranging

The Light Detection and Ranging (LiDAR) system is an airborne laser with a coherent beam at a precise wavelength, mainly used to detect and obtain 3D information of small objects.

In underwater environment, the main wavelengths used for the detection are the green-blue ones, thanks to their lower absorption in water. The amount of attenuation is significant, ranging from 0.2 dB/m to 1 dB/m, depending on the water clarity. However, this range can be modulated to enhance the capability of detection, rejecting underwater backscatter [35]. This system can conduct the survey at hundreds meters of depth (generally from 100 to 250 m) with a typical resolution in the order of decimetres [36] [37]. However, this system can provide the reconstruction of an underwater scene only from the air and cannot provide the detailed structure of single organisms.

2.2.1.3 Pulse Gated Laser Line Scanning

This method is the most common laser line scanning system, which uses the ToF principle. The target is illuminated by a short laser line pulse (typically each pulse has a duration of a few nanoseconds) and the receivers shutter is open only to capture the light returning from the target (Figure 6). In this way, the image contrast and the overall performances are improved [38].

The resolution and the accuracy depends on the length of the pulse. The maximum possible range is determined by the power loss of the received signal. Generally, this system can provide a millimetre accuracy and resolution [39]. The backscattered laser signal is affected by signal noise and the amplitude depends on the object´s surface properties, for example the reflective power and the topology. A commercial solution is available [40].

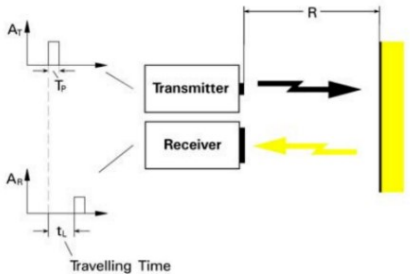

Figure 6 Pulse Ranging [41].

2.2.2 Modulation

In the frequency domain, the backscattered signal can be removed by discriminating it from the amplitude and phase of a modulated signal. The receivers are generally Photomultiplier Tubes (PMT) or Avalanche Photodiodes (APD) characterized by photon counters. These sensors are generally triggered during a time window, and integrates the incoming light.

Only low frequency components are efficiently transmitted, while high frequency components are lost. For underwater survey, the amplitude in frequencies are modulated in the order of GHz, thus requiring very sensitive sensors and accurate time scales.

The high dispersion in the sea water causes a fall of the coherent modulation/demodulation techniques at optical frequencies in underwater environments. So amplitude modulation is the only realizable modulation in underwater scenarios. Also in this case, the blue-green wavelengths are the most used (with a minimum absorption and scattering in water) by this technique for the detection in underwater environment [27].

2.2.2.1 Modulated Laser Line Scanning

The modulation of the transmitted signal can be used in LLS system providing several advantages. Indeed, image contrast is improved by reducing backscatter and the ambient light noise. Besides, the image sharpness is enhanced by decreasing forward blur/glow scatter [42, 43]. The modulated LLS provides better performance in turbid water and in bright solar background conditions, than the unmodulated one. The short wavelength of the signal provides accurate depth information by using coherent detection schemes.

2.2.3 Triangulation

The triangulation approach, as the name suggest is based on trigonometric properties of triangles, calculating the distance between two points not directly accessible of the same target. The drawback of this sensors is the necessity of an overlapping region for the emitter field of view and the receiver one [27]. Besides, this methods provides better resolution in shorter distances than in farther ones. In addition, the z resolution increases by increasing the distance between the two sensors used [44].

Different techniques use the trigonometric approach: the continuous wave laser line scanning (CW-LLS), which is a class of laser line scanning, and the structured light that are active optical methods and finally, the structure from motion and stereo vision that are passive optical methods.

2.2.3.1 Continuous Wave Laser Line Scanning

This subcategory of laser line scanning is characterized by a moving laser pointer that scan the object surface with the help of a rotating mirror. A CCD sensor is used to receive the return signal. By means of the camera sensor, this system can provide also colour information of the subsea object. The limitation is the different operational range of the two system: the laser has a larger minimum measuring distance (< 10m) than the camera (< 5m). For this reason, it is necessary to find a compromise between the laser scanning distance and the camera. The distance measure of the laser signal is limited by the wavelength that imposes a

maximum working distance of several tens of meters. In this case, the precision are around in the order of millimetres. Besides, this method scans in a few seconds the entire field of view. The number of points depends, among other factors, on the resolution of the camera and the acquisition speed provides up to one million points per second.

Overall, this laser-based technique presents a good trade-off between cost and accuracy, as well as an acceptable operational range. Some commercial solutions are available for 3D data gathering [45, 46, 47, 48].

2.2.3.2 Structured Light

Structured light is characterized by projected light patterns (often grids or horizontal bars) and a camera system [49]. The deformation of the patterns on the object surface allows to calculate the depth and 3D information of the detected objects. Depending on the resolution of the camera, this kind of system allows the digitization not of only one point at a time, but of several hundred thousand points.

Two major methods of stripe pattern generation have been established:

1. Laser interference method
2. Projection method

The first one uses two wide planar laser beam fronts that produce equidistant line patterns. By changing the angle between these beams it is possible to obtain different pattern sizes. If the camera and the laser are static, for this setting a motorized element is required. The triangulation process need to know relative position and orientation of the laser and camera systems.

In underwater environment, the range of scanning is limited up within 2 to 3 m in clear waters [50]: this is a necessary condition in order to obtain colour information too [51, 52, 53]. Besides, the resolution is lower due to the significant absorption and scattering (above 5mm at three meters) [54]. These systems can be mounted with a LED light to enhance contrast to detect the laser line (Figure 7). It is possible to find a commercial solution in [55].

On the other hand, the projection method projects an incoherent light on the object surface and basically works like a video projector. A typical measuring assembly consists of one projector and at least one camera (Fig. 7). For many applications, two cameras on opposite sides of the projector have been established as useful. Binary patterns are the most common used, because they are easy to achieve with a projector and simple to process but there are others different used in the literature [56]. Binary patterns generally uses a white light to be projected. In underwater scenario, grey and white coded patterns are usually projected and the accuracy of the 3D reconstructions reaches values lower than one millimetre, with high resolution [57, 58, 59].

The limitation of this system is the low acquisition time in real conditions and the missing data in occlusions and shadows due to the strong influence from illumination and contrast conditions.

Invisible structured light (e.g. infrared projectors), such as the Kinect, is also been tested in underwater conditions [60]. However, the infrared spectrum is almost all absorbed from a few centimetres and cannot reaches greater distances.

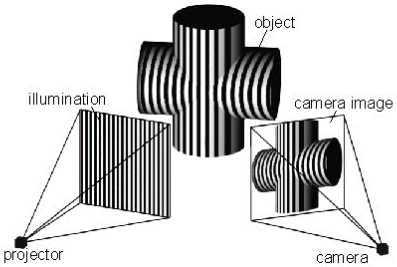

Figure 7 A scheme of a structured light scanning [61].

2.2.2.3 Stereo Vision

This technique is similar to the structured light methods but use only cameras (two or more) to capture, from different points of view, the scene or the object and render the 3D geometry. So, it is the passive version of structured light and is a simple and low cost method, by using only the cameras for scanning.

In the ideal case, the two cameras (right and left) are perfectly aligned and placed at the same height, at a given distance T. Both the cameras observe the same point P respectively from the projection centres O_l and O_r, and P is projected onto the respective projection plane at points p_l and p_r [62]. From the geometry of the stereoscopic system (epipolar geometry), it is possible to evaluate the horizontal deviation between the homologous pixels of the two images (disparity). Therefore, from the image pair, 3D coordinates of the features in the world can be computed by triangulation (Figure 8).

The depth *Z* is given by the following equation (2):

$$Z = \frac{f*T}{(x_l - x_r)} \tag{2}$$

Where: *f* is the focal length of the left and right cameras, *D* is the distance between the two cameras projection centres and $x_l - x_r$ is the disparity in pixels.

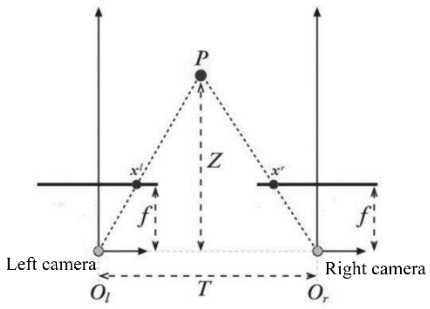

Figure 8 Triangulation geometry principle for a stereo system [63].

This technology is widely used to monitor coral reef ecosystem and to classify the different types of corals because of their low cost and simplicity, with a centimetre accuracy [64, 65]. However, the stereographic approach needs a textured scenes to achieve satisfactory results.

2.2.2.4 Underwater photogrammetry

The photogrammetric approach is getting widely used in underwater environments, especially to contribute in investigating the structural complexity of coral reef ecosystem and associated ecological processes [66]. It uses a monocular camera to reconstruct both depth and colour of the scene by taking only images around the object. This system uses the Structure from Motion (SfM) algorithm [67] in which, from each camera shots, image features are detected and matched between consecutive frames to know the relative camera motion and its 3D trajectory.

When objects are acquired at a distance less than 300 m from the camera, it is possible to define photogrammetry as "close-range". In this setup, the cameras acquire the volume or the area of the captured object to reconstruct. The location of these targets can be known as before or calculated after the images are captured if their shape and dimensions are known.

Image quality is a very important challenge in underwater photogrammetry. The main obstacle for the underwater photography is the drastic decrease of colour and contrast, increasing the depth: the longer the wavelengths of sunlight are absorbed by the water, the more the photos acquire a blue-green hue (Figure 9). The absorption is selective depending on the wavelength [68]: the first colour to disappear is red, which at 5 meters depth is reduced by 95%. The colour loss not only increases in depth, but also because of the distance, so that objects far from the camera are blurred and faded. These issues will be addressed and elaborated on Chapter 4.

Another factor that negatively affects the image performance is particles suspension in the water. However, this effect is very small in clear water, as in tropical coral reefs, and photos are clear and similar to the surface environment [69].

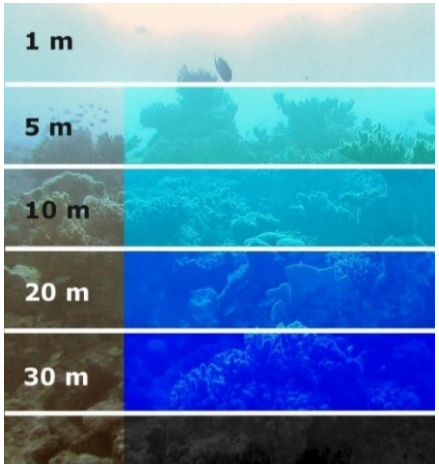

Figure 9 Light absorption in underwater environment that grows gradually with depth.

In Table 1, all the described technologies are summarized. The general differences in terms of accuracy and resolution are highlighted. It is possible to see that underwater photogrammetry is the easiest and low cost system to obtain a good submarine reconstruction in low depth water. Moreover, the usage of a camera makes it possible to acquire the colour information of the scene.

3D Techniques	Method	Accuracy	Resolution	Range	Weakness
Sonar	ToF	cm	Low	Long	High cost
LiDAR	ToF	< m	Low	Long	Safety constraint
PG-LLS	ToF	mm	Intermediate	Medium	Forward backscatter
M-LLS	Modulation	cm	Intermediate	Medium	High dispersion
CW-LLS	Triangulation	mm	Intermediate	Medium	High cost
Structured Light	Triangulation	< mm	High	Close	Missing data in shadows
Stereo Vision	Triangulation	cm	Intermediate	Close	Low data acquisition rate
Underwater Photogrammetry	Triangulation	< mm	High	Close	Needs artificial illumination

Table 1 Some main characteristic of the different scanning methods.

3. Testing the Laser-Based Method for Underwater Application

In the first year of this research, a novel laser-based approach for coral surface reconstruction has been tested. The coloured 3D models are acquired in water by RGB-ITR (Red Green Blue–Imaging Topological Radar) Laser Scanner prototype that was developed for terrestrial applications. This system is chosen because integrates the distance measurement of the target points with the colour information, using amplitude modulation of three monochromatic laser sources (red, green and blue wavelength). The one performed in this thesis represents the first tentative to bring this technology in underwater applications, therefore issues in achieving this goal are highlighted in this chapter.

3.1 Acquisition System: the RGB-ITR Laser Scanner

RGB-ITR system is the 3D colour laser scanner prototype realized by ENEA[1] Artificial Vision laboratories. The system can be considered a combination of a 3D scanner and a tristimulus colorimeter [70].

It is characterized by two main modules: a passive module, composed by the system optical head, basically including the launching and receiving optics; an active module, which includes three monochromatic laser sources at 650 nm (red), 532 nm (green), and 450 nm (blue) wavelengths, modulators, detectors, and all necessary electronics for data collection and processing. The two modules are physically separated and optically connected by means of optimized optical fibres. This enables the use of the system in hardly accessible or even hostile environments [71].

The three laser points can scan the interested area by means of a mirror anchored at a rotating metallic box. The angle of view of the system is $80^0 \times 310^0$, with a point-to point precision of 0.002^0. This resolution can provide a structured and dense point cloud in the working range of the scanner, which is from 3 to 30 meters.

It can be classified as an M-LLS (Modulated Laser Line Scan) because the amplitude of each wavelength is modulated with a high and a low frequency: the frequency modulation is used to obtain a higher precision measurement in a smaller range and the low frequency modulation to measure the distance in a bigger range, between the centre of the optical head and the target. The simultaneous collection of distance and colour information are extracted respectively through phase-shift and amplitude of back-reflected waves by the target surface.

In detail, the distance information is derived from equation (3):

$$D = \frac{v\Delta\phi}{4\pi f_m} \tag{3}$$

where *fm* is the modulation frequency, $\Delta\phi$ the phase difference between the reference modulating wave and the signal back-reflected by the target, and *v* the light speed in the medium [72].

[1] Italian National Agency for New Technologies, Energy and Sustainable Economic Development

Instead, the colour information is elaborated by a lock-in amplifier Stanford SR-844. The raw data are the result of the amplitude of each back-reflected modulating signal from the target, expressed in Volt. The ranges for each channel are about 0.1–100mV, then converted from analog to digital signals, by three 16-bit ADC.

Before merging the distance and colour information, it is necessary to calibrate the system by moving a certified white target (Spectralon STR-99-020, diffuse reflectance 99%), at several distances and striking it with the three laser sources [73]. The normalized image is given by the ratio between the amplitude value of the three wavelengths reflected by the target surface and the white calibration target.

For each channel the measured reflectance factor of the target is given by (4):

$$R_d(\lambda_i) = \frac{V_d(\lambda_i)}{V_d^{white}(\lambda_i)} \cdot R^{white}(\lambda_i) \tag{4}$$

where: $R_d(\lambda_i)$ is the measured reflectance factor at the distance *d*, $R^{white}(\lambda_i)$ is the certified spectral reflectance factor of the white target used in this measurement and $V_d(\lambda_i)$ and $V_d^{white}(\lambda_i)$ are the respectively voltages (in mV) (Figure 10).

The software is composed by two main interfaces: the first one, called ScanSystem, controls all the aspects of scanning and data acquisition. It is possible to change the scanner parameters, as for example the modulation frequency, gain filters or sampling frequency of the three channels, so to guarantee the best solution for the acquisition of the scene under investigation. The second one, called ITRAnalyzer, is able to build, analyse, and export all the data.

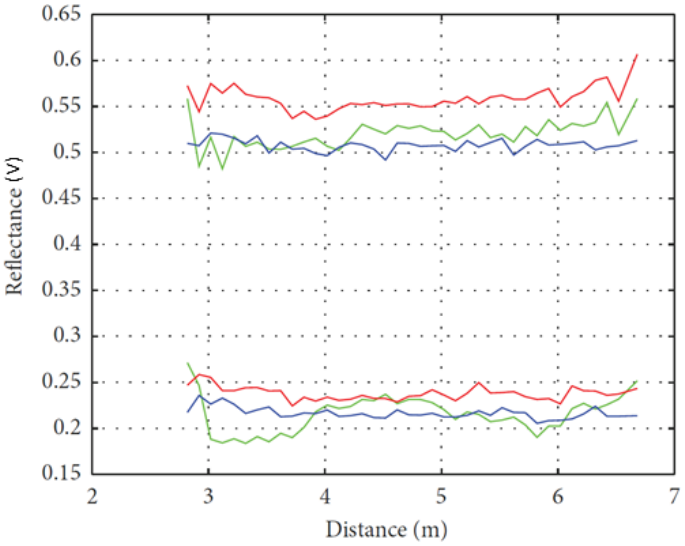

Figure 10 An example of calibrated reflectance values of the three channels: up there is the back-reflected signal of a grey target at different distances, below the back-reflected signal of a black one.

3.2 Acquisition Procedure

In literature, it is possible to find archaeological studies in which 3D information is obtained by means of this prototype [74]. These studies have shown the considerable potential of this approach, also highlighting several critical issues.

In the frame of this thesis, the performance of the system in the ideal condition of terrestrial scanning was further elaborated, i.e. expanding its features for detecting objects in water. The experimental tests, conducted at the Research Centre (ENEA), were performed in different measurement conditions, by using different terrestrial and air datasets. The case studies presented in this chapter concern the survey of small and medium-sized objects with different 3D morphological complexity. The obtained 3D models were compared and analysed, to demonstrate the feasibility of the instrument to accurately reproduce the underwater scenes (objects) in 3D.

3.2.1 Case study: Terrestrial application

The first case study concern the dataset consisting of the three samples with different shape complexity: a marine sponge, named *Ircinia Campana (IC),* was the low complexity target; while a natural small scleractinian ramose coral colony, named *Pocillopora Coral (PC),* and a red coral, named *Corallium Rubrum (CR),* were used for the medium and high complexity respectively (Figure 11).

The acquisitions are carried out by placing the three samples at 4m from the optical head on rotating supports (Figure 13). The three lasers were modulated with a high frequency of 190MHz and a low frequency of 10MHz and the spot size was about 0.2 mm.

To set the scanning scene, the Scan System software is used. This dialog interface can allows to move manually the scanning mirror, in order to set the acquisition scene. It is possible to divide the acquisition process in different sub-scan with different scanning-parameters customization, for acquiring complexity scenes. At each scan, the samples are rotated by 45^0 to acquire the point cloud from different angles, for a total of 4 overall scans.

Each scan has a duration of 80min, so acquisitions were performed in different days. In the scene, the white reference target is placed near the samples, in order to colour correct the texture in the post-processing phase.

Figure 11 From right to left: the three adopted samples with growing complexity structure.

3.2.2 Case study: Underwater application

The second test was performed on a dataset that included only the high and medium complexity targets. The first one (*CR*) is immersed in an aquarium with relatively clean water and a black background was used to avoid laser dispersion due to glass.

The second one (*PC*) is immersed in a matt bucket to avoid dispersion due to the glass, with the laser pointed perpendicularly in the bucket. In this latter case, the laser devolved directly into the water and there is not the air-glass interface as in the first case, where light waves have to pass three different kind of media (air-glass-water).

As for terrestrial scanning, the three lasers were modulated with a high frequency of 190MHz and a low frequency of 10MHz and the spot size was about 0.2 mm. They were both placed about 1.70 meters from the centre of the optical head.

In this case study, the samples are acquired only with a frontal scan and are not rotated as the previous acquisition.

Figure 12 The CR immersed in the aquarium and the PC in a matt bucket.

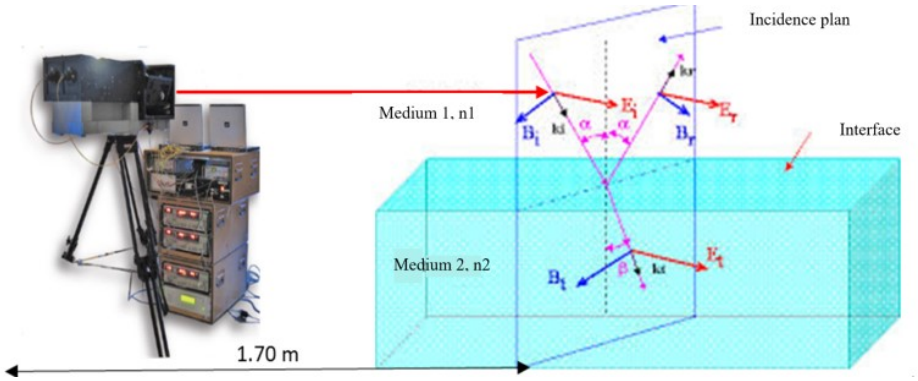

Figure 13 Configuration of the underwater acquisition with the RGB-ITR

3.3 Image Processing and 3D Reconstruction

The acquired data was processed with Itr Analyzer interface, which enabled 3D point cloud reconstruction. The procedure of image processing are characterized by the following main commands:

- *"Open ITR project"*: to load the acquired images as *Matlab* files (.mat format) or from desktop (.prj format). The set of uncalibrated images are characterized by both the colour and the texture information that have to be calibrated.
- *"Data analysis":* for a preliminary analysis of both colour and distance information of the acquired data.
- *"Image normalizer"* : to change the range of pixel intensity values by selecting several points on reference target;
- *"Complete mesh":* to generate and visualize the surface of the 3D object;
- *"Create mask":* to select a threshold from histogram of the acquired scene, delating the pixels of the background;
- *"Export mesh"*: to save the surface of the 3D object (.ply format) with texture;
- *"Register mesh":* to register meshes obtained by different point-of-view scans. This command is used only for the first dataset where the samples are rotated and acquired from different scans. On the contrary, in the second dataset the samples are acquired only from one scan.

With the open source system, called MeshLab, the object's surface was edited, cleaned and filtered. In Figure 14, the two modules for acquisition and data processing are shown.

(a) (b)

Figure 14 User interface of ScanSystem (a) and ITR Analyzer (b) software modules.

4. Implementation of a Colour-Correction Algorithm for Underwater Photogrammetry

This Chapter is an introduction of the work related to the adopted photogrammetric approach. Before describing the procedure and the results obtained by means of this method, it is very important to illustrate the pre-processing step implemented for the restoration of the underwater images in the frame of this thesis.

It introduces a main contribution in the field of image-based scanning methods, not only to determine the real colour of the acquired object but mainly to restore the colourcast and illumination of the underwater scenes, improving the image point matching in the 3D reconstruction. As results, the degraded images, due to the different exposure of natural lighting and to the light absorption in water condition, are balanced and enhanced with high details and good quality.

The Chapter begins with a focus on the description of the main issues that cause poor visibility in aquatic scene. In addition, a review of the adopted colour corrections methods (for reducing such issues), is performed. Finally, the proposed method is described, highlighting how the proposed method contribute in addressing the encountered issues.

4.1 Image Processing Issues in Underwater Applications

The attention for underwater image analysis is increasing in order to improve the underwater exploration, the habitats monitoring and the species detection and recognition [75, 76]. However, obtaining high quality images in underwater environment is a challenging task, because of the limited range of visibility, the low contrast, the non-uniform lighting, the bright artefacts, the noise, the blurring, and the diminishing colour with the proportional increase of the greenish or bluish.

The main reason of these phenomena is light attenuation caused by absorption and scattering. The first one causes a reduction in colour information because light propagation is partially lost, while the scattering effects cause change of the direction of radiation due to the different density of the medium and this translates in blur and reduction of the acquired image size.

In general, in clear open waters, light intensity has a rapid exponential loss depending on the colour spectrum wavelength [77]. Indeed, for a light beam with a wavelength λ traveling through water for a distance d, if $\eta(\lambda)$ is the attenuation coefficient defined by:

$$\eta(\lambda) = a(\lambda) + b(\lambda) \tag{5}$$

where $a(\lambda)$ is the volume absorption coefficient and $b(\lambda)$ is the volume scattering coefficient depending on the angle $\varphi \in [0, \pi]$, both measured in [m^{-1}], the loss is given by the following equation:

$$E\,(d,\lambda) = E\,(d_o,\lambda)\cdot e^{-\eta(\lambda)d}\ [\mathrm{Wm}^{-2}] \tag{6}$$

where $E\,(d_o,\lambda)$ and $E\,(d,\lambda)$ are the irradiance before and after traveling the distance d through the water.

From visible spectrum, the first wavelength subject to the absorption is the one at the longest wavelengths, so the red colour, which is reduced to $1/3$ of its intensity from 1 m, is the first one to be lost, while blue and violet colours are absorbed last (Figure 15). Moreover, due to the different crossed media, refraction of light occurs depending on the optical density of the media. The Snell's law reporting the relationship between the incident angles θ_1 and the refractive angles θ_2 is expressed by (14):

$$\frac{\sin\theta_1}{\sin\theta_2} = \frac{n_2}{n_1} = \frac{v_1}{v_2} \tag{14}$$

where: n_1, n_2 are the refractive index of the two media and v_1, v_1 are the respective speed of light.

The obtained vision suffers from a degradation of the colours, of the image focus, and therefore of the sharpness, and a distance reduction of the 25%.

For all these reasons, the performances of the underwater imaging systems are degraded and some strategies to compensate the poor visibility and the colour dispersions are developed.

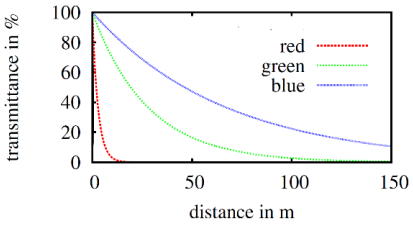

Figure 15 Transmittance for the three wavelengths corresponding to the RGB colour channels.

There are several methods in literature, adopted for colour correction of underwater scenes at diving depth, useful to preserve a significant part of sunlight and distinguish the different natural colours. Typical models are based on the physical principles as the Beer's law [78] and the Jaffe-McGlamery image model [79]. However, these methods require to calibrate the necessary parameters of the physical model in the local water body [80].

Other methods correct the underwater scene by exploiting polarization filters [81, 82] or enhancing images with a contrast stretching of RGB channel [83]. The limitation is that the polarization methods process several images with different degrees of polarization and this can be a problem for the setup of the camera. While only the contrast enhancement does not solve the problem of the different lighting conditions.

Other works provides the correction of non-uniform illumination by using homomorphic filtering [84, 85, 86, 87]. The colour scene is improved but the overall image visual quality is poorly increased.

In [88, 89], the Integrated Colour Model (ICM) and the Unsupervised Colour Correction Method (UCM) are proposed. The colour images are enhanced by a global stretching in RGB and HSI colour space. The overall contrast performances of the output images for both

techniques increase, but not much difference can be observed in the output images using both techniques, because there is any improvement of the colour cast of the aquatic scene.

In [90], the mentioned techniques are modified by stretching two different image contrasts (brightness and darker areas) in a mid-point with respect to the Rayleigh distribution. Also in this case, no improvement in the image colour is observed and the blue-green illumination is retained.

Other methods for restoring the illumination of the underwater images are performed in [91, 92]. The enhancement of the images contrast is combined with the white balancing techniques to correct the intensity colours.

In the frame of this work, the proposed method aims to extend the colour correction process proposed in [91], by introducing the gamma correction step that reduces the brightness distortion, without generation of additional artefacts and making the illumination of the dataset uniform. The utility of this approach is proved for the task of the 3D reconstruction by matching images with local feature points.

4.2 Proposed Method for the Colour Correction

In this section it is described the colour correction method proposed for underwater imaging. The idea of the proposed method is to restore both the contrast, the intensity and the brightness of images by means of an automatic algorithm. The Contrast Limited Adaptive Histogram Equalization (CLAHE) approach [93] is initially applied to enhance the local image contrast. It is followed by Grey World balancing [94] that performs restoration of the colourcast and finally by gamma correction [95] that restores the brightness for dimmed underwater images.

It is necessary to remind that in this work the scenes are intentionally not uniformly illuminated by artificial light sources, but acquired only with the natural illumination. For this reason, it is possible to assert that these three-step procedure corrects the colour of the scene, successively reconstructed through the Structure from Motion (SfM) approach, improving the matching point recognition and classification of the object under varying illumination.

This image pre-processing procedure is carried out by means of the implementation on ©Matlab software of a colour correction algorithm. The block diagram of the method is shown in Figure 16.

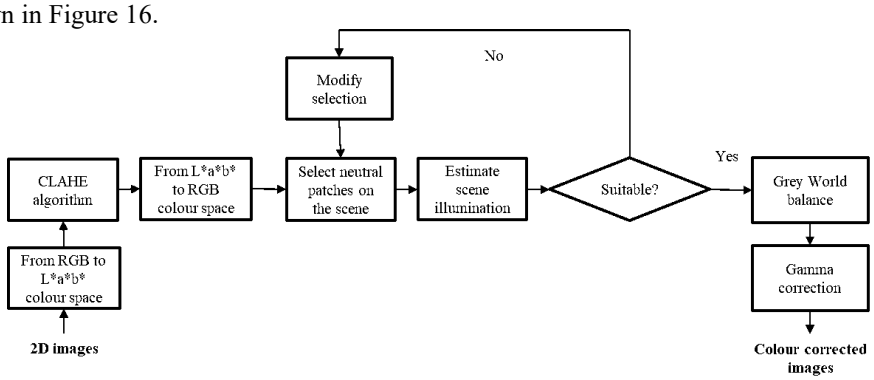

Figure 16 Block diagram of the proposed method.

4.2.1 Contrast Enhancement Technique: CLAHE Algorithm

This algorithm is the extended version of the Histogram Equalization (HE), which is one of the well-known method for enhancing the contrast of the images, performing a uniform distribution of grey levels on the entire image, adjusting the ratio between the highest value (brightest point) and the lowest value (darkest point). However, HE operates on the whole region, and the risk is that the local details has smaller probability to be enhanced.

On the contrary, CLAHE operates on local regions of the image, called 'tiles', rather than the entire image. Precisely, each pixels region is cut and the Cumulative Distribution Function (CDF) is performed for each individual tile.

Given a grey scale region with grey levels in the range [0, L-1], the CDF can be described as follows (9):

$$S = (L-1)\sum_{j=0}^{l}\frac{n_j}{n} \tag{9}$$

where: n_l is the frequency of occurrence of the corresponding grey level and n is the total pixel population in the region. After equalization, to remove artefacts in tile borders, bilinear interpolation is applied. In other word, the improvement of the quality is due to the 'stretching' of the range of intensity values.

In the proposed method, the contrast is limited to avoid amplifying any noise that might be present in the image, especially in homogeneous areas. This is performed by transforming the image from RGB to the L*a*b* colour space, where the 'L*' component has the intensity values on which the algorithm operates. The luminosity values can span a range from 0 to 100, so they are scaled to [0 1] range before applying the three contrast enhancement techniques. Manipulating the luminosity, only the intensity of the pixels is changed, while the hue of original colours is preserved. After the CLAHE algorithm, the image is returned back to the RGB colour space.

4.2.2 Colour Balance Adjustment

Grey World is one of the white balancing techniques, which assumes that the average of all the colours in the scene are grey.

This algorithm is characterized by two main steps: the first one is to estimate the illuminant, the neutral reference point, by picking one or more pixels in the image that look grey or white. Secondly, the colour cast is compensated based on the estimated illuminant value. The average of the selected colours is used as reference for the scene calibration, excluding under- and over-exposed pixels. This is implemented on the RGB colour space, as mathematically expressed in the following expression:

$$R_{avg} = \frac{1}{(m)(n)}\sum_{x=1}^{m}\sum_{y=1}^{n}R(x,y) \tag{10}$$

$$G_{avg} = \frac{1}{(m)(n)}\sum_{x=1}^{m}\sum_{y=1}^{n}G(x,y) \tag{11}$$

$$B_{avg} = \frac{1}{(m)(n)}\sum_{x=1}^{m}\sum_{y=1}^{n}B(x,y) \tag{12}$$

where: *m* and *n* are respectively the rows and columns pixels of the image and *R, G* and *B* are the original colour, in the three channels colour space, of the selected points.

Then, the hue of the scene is corrected with the chromatic adaptation according to the illuminant estimation.

The main goal of this adjustment is to render correctly the neutral colours changing the overall mixture of hue in the images. In other word, colour balancing provides the same colour of an object in images under different lighting conditions.

4.2.3 Gamma Correction

As a final step in the proposed method, the brightness of the images is corrected. The illumination value estimated on the illuminant in the colour balance step, is used also for the gamma correction procedure. Indeed, gamma correction is a function that maps luminance levels in order to enhance the brightness. In particular, the mean of the RGB values on the illuminant is used as gamma value to restore the brightness.

In other word, gamma specifies the shape of the curve describing the relationship between the intensity values in the original image and the output image. For a mathematical analysis, this relationship can be described by the equation below (13):

$$y = x^{\Upsilon} \tag{13}$$

where: y is the input and x the output intensity values.

Gamma can be any value between 0 and infinity. When the relationship between the input and output is linear, so for $\Upsilon=1$, the intensity values match perfectly. For $\Upsilon< 1$, the mapping is estimated toward higher (brighter) output values. On the contrary, for $\Upsilon> 1$, the mapping is weighted toward lower (darker) output values.

In Figure 17 the transfer function of gamma correction is shown for varying values of gamma.

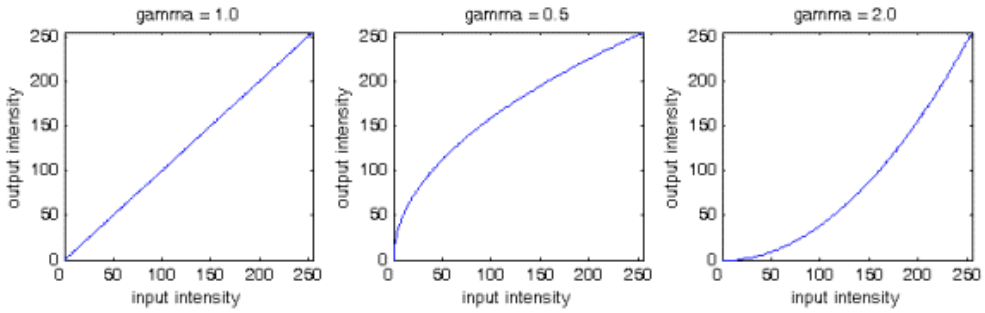

Figure 17 Varying gamma values

5. Evaluation of the Photogrammetric Method for Underwater Application

In the previous chapter the main challenges tackled in underwater imaging and the algorithm implemented to recover the colour information lost, due to the light absorption, are shown.

In this Chapter the focus is on the photogrammetric approach, acquisition strategy used widely for the development of this thesis, and the SfM algorithm that is commonly coupled to the photogrammetry to have the necessary information for the 3D reconstruction of the underwater scene. In particular, the optics used to obtain detailed 3D models of small-sized objects are explored and the case studies addressed in this thesis are listed.

5.1 Acquisition System: Camera for Detailed Scanning

As regards experiment testing, the equipment is carefully selected in order to obtain a comparison between different optics. In particular, two different camera bodies are adopted: the GoPro Hero 5 modified and the Nikon D5600.In conjunction with the camera bodies, different kind of lenses are used. Indeed, in the frame of this thesis, the research of the best optical solution for underwater acquisition is carried out: it is very important to adopt the right lens according to the scene or subject to shoot.

The different optical performances of the two cameras are due to the different features (Table 2): GoPro is a typical commercial camera, generally with a wide angle lens, while in the frame of this work the peculiarity is the adaptation of two fixed lenses that can be mounted with optional M12, F, CS and C-mount adapters. On the other hand, Nikon is a Reflex with a mid-range of view and a better performance sensor. The main differences between the two cameras are the sensor resolution, which for Nikon (24.2 MP) is higher than the GoPro (12 MP), the sensor size that for Nikon is a 'full frame' sensors (1.5x), the similar size as traditional 35mm format film, and for GoPro is a 'cropped' sensor (5.6x), smaller than full frame, and the ISO value, higher for Nikon that allows better performance in low light conditions.

Camera features	GoPro Hero 5	Nikon D5600
Sensor type	Cropped sensor	Full frame
Sensor resolution	12 MP	24 MP
Sensor size	5.6 x	1.6 x
Base ISO	100	100
Maximum ISO	3200	25600

Table 2 Cameras features

For what concern the lenses used in this study, four different kind are selected according to their focal length and are:

- a C-mount lens, with 16mm focal length, generally used for industrial applications;
- two F-mount lenses, respectively with 60mm and 90mm focal lengths, designed especially for close-up photography;

– a zoom lens AF-S with 18-105 mm lens.

In this way, the camera offers wider-angle shots with the first one (rectilinear) lens, or a narrower field of view with the second ones (macro lens), which can provide professional and detailed results (not achievable with standard lenses) and higher versatility. The zoom lens are very useful in particular in underwater condition, where the shooting distance cannot be fixed, although fixed lens has better optical quality than the zoom lens that instead provides more flexibility.

Another main difference between the two camera systems is the underwater housing, adopted to confine them in order to avoid electric shortening or implosion. The underwater housing introduces one more cause of geometrical distortion. Indeed, the light is first traveling through water, then glass, and finally air before it reaches the actual camera sensor.

For Nikon, the camera case is characterized by a rigid body with full automatic controls and a piece of glass formed as a 'dome port'. Since refraction depends on the angle between the entering ray and the normal of the interface, in case of a dome port underwater housings, the light rays are not refracted because all rays are parallel to the interface normal.

On the contrary, GoPro camera and lenses are confined in a plastic case with a 'flat port' where the light is almost all refracted. Indeed, only the light rays that pass perpendicularly through the interface are not deviated. (Figure 18).

The most known consequence is that the field of view of the lens mounted on the camera is preserved in case of a dome port and reduced of a factor (almost equal to the refractive index) for the flat port [96]. Nevertheless, if the centre of the dome is not aligned with the entrance pupil of the lens, modifications of field of view and distortions may be introduced.

The comparison between the different equipment used, is fundamental in order to choose the best solution for investigating detailed 3D models in underwater scene.

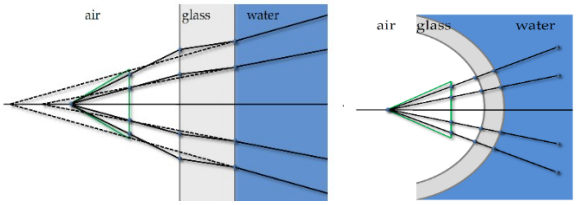

(a) (b)

(c)

Figure 18 Difference between the refraction due to a flat port (a) and a dome port interface (b) and the underwater housing used in the test laboraotry.

5.2 Acquisition Procedure

Data acquisition exploits the principle of photogrammetry: the quantities that need to be related are the 3D coordinates (X, Y, Z) of the object, the 2D coordinates (x, y) of the image and the orientation parameters.

The procedure is carried out by capturing images from different viewpoints. Then, the orientation parameters provide the match between the image and the object space and, when the camera positions are defined, the transformation from 2D image coordinates to the corresponding 3D world coordinates characterizes the shape and size of the detected object.

The algorithms used for the 3D reconstruction are based on the SfM approach and are subjected to developments and continuous changes, exploiting different information from the images, such as shadows (shape from shading), texture (shape from texture), silhouette (shape from silhouette) [97, 98]. The SfM allows the reconstruction of a sparse points cloud from unsorted images [99] and determines the corresponding characteristics in the different images, to calculate the intrinsic and extrinsic parameters of the camera (self-calibration) through different operators of interest. These operators have to be as much as possible invariants with respect to the variations of scale, rotation, translation and the lighting change and points of view, such as the SIFT (Scale Invariant Feature Transform) [100] and the SURF (Speeded Up Robust Features) [101].

Recently, the SfM is combined with 'dense image matching' algorithms to improve 3D reconstructions by producing a dense points cloud. Generally, they are classified in 'Area Based Matching' (ABM) and 'Feature Based Matching' (FBM), often merged [102].

The ABM algorithms reconstruct the dense points cloud by means of the intensity pixels values and the matches are found by comparing two small portions of images (image patches), one kept fixed, called *template matrix*, and the second named *search matrix*, is moved to search for the corresponding area on the other image [103]. The comparison is performed with 'cross-correlation' and 'least squares matching' criteria, minimizing the grey level differences between the template and the matching window. The ABM present some problems related to the occlusion, different brightness and repetitive of the textures. For this reason, it is clear that, since the image pre-processing implemented within the research activity restores the pixel intensity values of the stereo pair, is extremely useful to address the mentioned issues, improving and increasing the dense images matching obtained by means of this algorithm.

On the other hand, the FBM algorithms first search the features (angles, corners, edges etc.) in the stereo images and then analyse the correspondence. Also in this case, the contrast enhancement in the colour pre-processing is an important step to increase the features extraction.

The SfM approach is implemented in open-source software (Blunder and PMVS, VisualSFM, Apero, etc.), in commercial software (Photoscan, Photomodeler Scanner) and also in web applications defined '3D web-service' (ARC3D, Autodesk 123D Catch, Cubify, My3Dscanner etc.) [104].

The work of this thesis is mainly focused on the realization of the 3D models of small-sized objects, with the aim to investigate the performance of the different applications (in-air and in water conditions) in relation to the quality and metric accuracy of the final results. The 'Photoscan' low-cost software was used for this purpose. The datasets are obtained with the different cameras and setting conditions (number of images, resolutions, setting distances,

etc.) and are related to a blanching coral named *Pocillopora Verrucosa* (*PV*), placed before in air and then inside test tub.

A cube with white and black reference squares is placed under the sample and framed in all the acquired images to ease the colour reconstruction procedure. Indeed, as mentioned before, all the images are pre-processed with the colour correction algorithm described in Chapter 3, before the reconstruction process.

5.2.1 Case study: Terrestrial Application

The first case study was performed using images taken around a ramose coral colony placed on a cube, in-air condition and illuminated by ambient light (Figure 19). The acquisitions were carried out by means of the two cameras, GoPro and Nikon, with the different optical lenses, respectively 16mm and 60mm lenses for the first one and zoom lens for the second one, in order to realise the 3D models with various levels of details. The images are acquired with random positions of the cameras and without using a tripod, except for the 60 mm that requires greater stability (manual focusing). The number of shooting varies between the 20 and 50 photos. The lenses are set up with a medium aperture and the set of images are collected by convergent and stereoscopic sequences, taken by tilting the cameras in order to have a good coverage of the object.

The dimensions of the acquired areas vary from a minimum of 20 cm^2 to a maximum of 50 cm^2, depending on the shooting distance. The distance depends on the focal length used: is about 50 cm for the 16 mm lens, about 2 m for the 60mm lens and variable for the zoom Nikon lens.

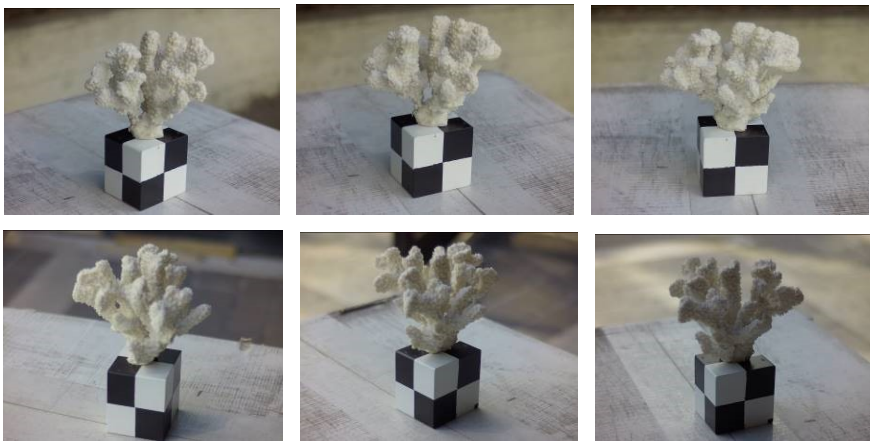

Figure 19 An example of photos of the PV acquired in-air condition and with different lighting illumination.

5.2.2 Case study: Underwater Application

The second case study regards the acquisitions in water conditions. Before dipping the cameras into the water, only the sample was immersed in an aquarium, for a first assessment of the feasibility of the survey. Then, each camera is confined in the appropriate case and immersed.

5.2.2.1 First dataset: Target immersed in water

This first dataset is characterized by a test water tank designed with eight-sided, in order to reduce the distortion due to the glass (Figure 20). Indeed, only three photos for side are taken to make sure that light rays pass approximately perpendicular through the interface and are minimally deviated. The aquarium is filled with clean water to avoid suspended particles that could causes absorption and refraction. However, the effect of the water on the glass pane causes air bubbles that generate a loss of sharpness in the acquired photos (Figure 21). As for the dataset defined for the terrestrial application, also in this case the sample is acquired with ambient light condition and with different shooting distances.

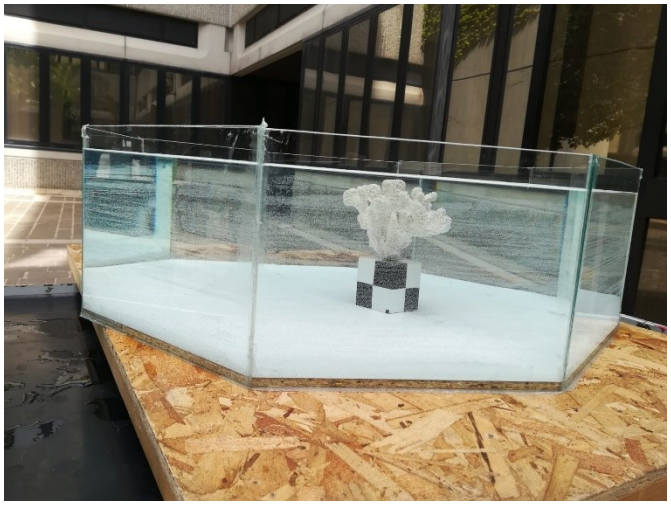

Figure 20 Set up of the described dataset

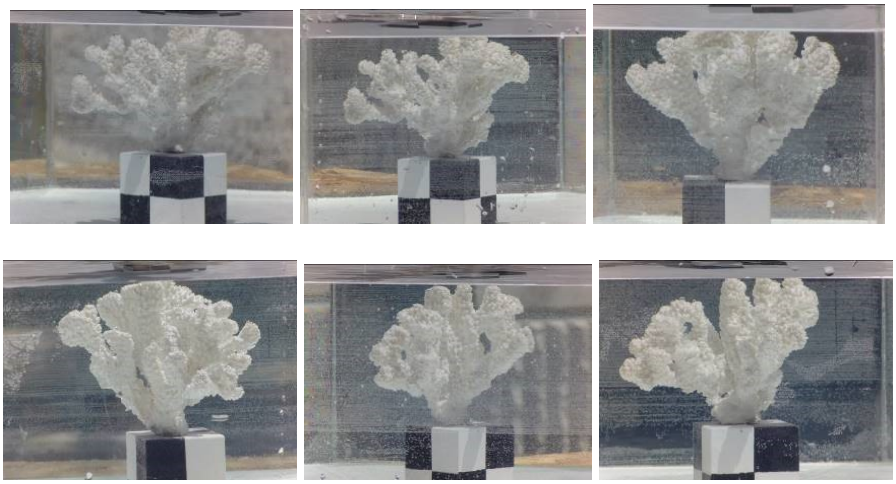

Figure 21 An example of images acquired with sample immersed in the aquarium.

5.2.2.2 Second dataset: Target and camera immersed in water

The second test is performed in a test tank, size 245 x 130 x 120 cm, filled with about 50 cm depth of relatively clean water (Figure 22). As described in Section 5.1, the GoPro is closed in a plastic case with a flat port, while for Nikon a rigid body with a dome port is adopted (Figure 18). For this acquisition, the 60 mm lens is replaced with the 90 mm lens with similar performance, but with the possibility of autofocus. In addition, it was connected with the Nikon body to allow also the control of manual focus and all the other functions. In addition, in this way the shooting angle and the chromatic aberration are restored. Moreover, since the tank is small, the sample was acquired through this lens by rotating it every 45°. In the processing phase, the entire 3D model is obtained by merging the four stereoscopic scans. While for the 16 mm and the zoom lenses the acquisition procedure is the same as in the previous cases, because the shooting distance is shorter.

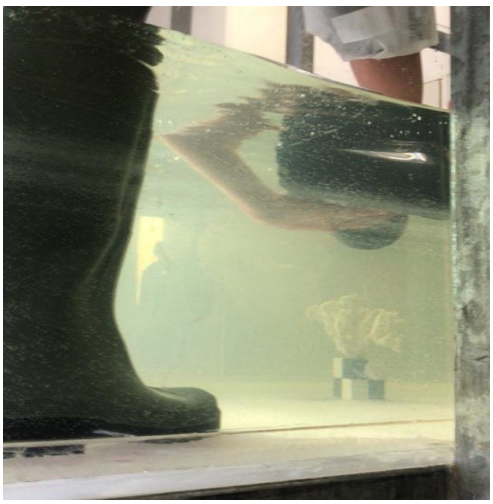

Figure 22 Data acquisition with sample and camera immersed in water.

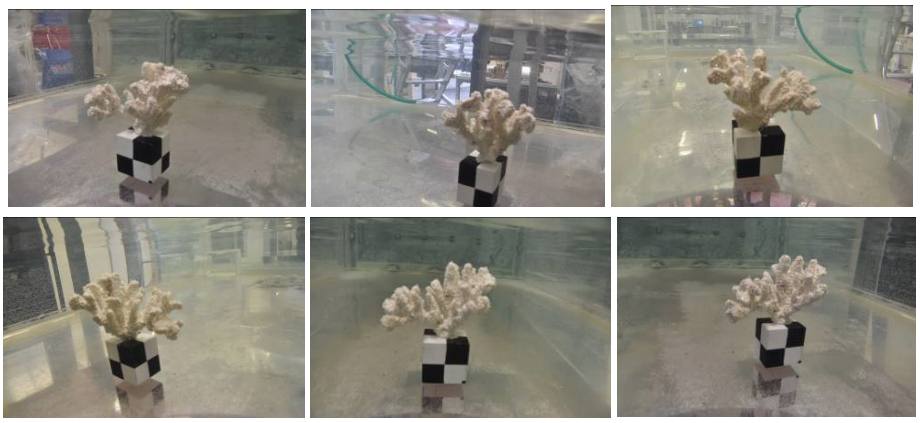

Figure 23 An example of sample acquired in water.

In Table 3, Table 4 and Table 5, the different acquisition parameters are summarized for the three datasets. The number of images, the acquisition times and the shooting distances obtained by the three cameras and lenses are shown.

	DATASET 1		
	N. images	**Time (min)**	**Distance (mm)**
Gopro+16mm	41	5	~500
Gopro+60mm	48	12	~1950
Nikon+zoom lens	18	3	Var.

Table 3 Acquisition parameters for sample acquired in air condition.

	DATASET 2		
	N. images	**Time (min)**	**Distance (mm)**
Gopro+16mm	24	6	~500
Gopro+60mm	24	14	~1850
Nikon+zoom lens	24	5	Var.

Table 4 Acquisition parameters for sample immersed in the aquarium.

	DATASET 3		
	N. images	**Time (min)**	**Distance (mm)**
Gopro+16mm	23	9	~300
Nikon+90mm	41	16	~1600
Nikon+zoom lens	30	10	Var.

Table 5 Acquisition parameters for sample and cameras immersed in the water tank.

5.3 3D Reconstruction and Modelling

The commercial ©PhotoScan software, exploiting the SfM method, is used to obtain the 3D models. The workflow is completely automatic and includes image orientation, reconstruction and texturing of the 3D model. The models are exported in '.ply' or '.stl' format, exploitable in other external software. All processes can be executed with various precision levels and many parameters can be set to improve the final results.

The first step is 'Align photos' to identify the accurate key point correspondence on the set of images and obtain a sparse point cloud in the local 3D coordinate system. By setting certain parameters, it is allow to adjust the quantity of the extracted points and the processing time for each image. In this phase, the position of the camera for each image is found and the camera calibration parameters are automatically determinated (self-calibration). To avoid errors storages at each iteration and therefore to improve accuracy of the 3D reconstruction, the 'bundle adjustment' is applied. Finally, to achieve good reconstruction results it is necessary to mask all irrelevant elements on the source photos (background, accidental foreground, etc.).

The second step is to 'Build dense cloud' to intensify the sparse point cloud. Based on the estimated camera positions the program calculates depth information for each camera to be combined into a single dense point cloud. Since the geometry of the object to reconstruct is complex and with numerous small details, the filter is set to the 'delicate depth mode';

The last two steps consist in building the mesh and the texture to reconstruct a 3D polygonal surface on the dense point cloud and apply textures from images to the geometry.

5.4 Geo-Referencing and Scaling Procedures

After the 3D reconstruction step, the models are georeferenced by real world coordinates of eight points on the scene. These reference points, named Ground Control Points (GCP), are selected on top of the cube and provide a first assessment of the computed models.

The Root Mean Square Error (RMSE) for X, Y and Z coordinates of GCP locations are calculated as follows:

$$RMSE_x = \sqrt{\sum_{i=1}^{n} \frac{\Delta x_i^2}{n}} \tag{14}$$

$$RMSE_y = \sqrt{\sum_{i=1}^{n} \frac{\Delta y_i^2}{n}} \tag{15}$$

$$RMSE_z = \sqrt{\sum_{i=1}^{n} \frac{\Delta z_i^2}{n}} \tag{16}$$

where Δx_i , Δy_i , and Δz_i are the differences between reference coordinates and the coordinates determined from the point cloud, and n is the number of points in the set.

Then, the relative distances between the GCP selected on the reconstructed scene are calculated and compared with distances measured by means of a digital calibre, in order verify and evaluate the scaling of the models (17).

$$d(GCP_i, GCP_j) = \sqrt{(x_i - x_j)^2 + (y_i - y_j)^2} \tag{17}$$

where x_i, y_i and x_j, y_j are respectively the X and Y coordinates of two consecutive points.

6. Results and Discussion

In this Chapter the results related to the experimental test carried out by means of the different scanning methods and systems are shown. It is possible to see the differences between the laser-based and image-based technologies adopted for the scan, in terms of feasibility, identifying the strengths and weakness during the application in underwater environment. In addition, a section (6.2) of the results is dedicated to the colour correction results performed by the implemented algorithm.

6.1 RGB-ITR Laser Scanner Results

The results show the 3D models obtained by means of the laser scanner in the ideal condition of in-air scanning compared to the 3D models of the samples acquired in water. In addition, some examples of data analysis with ItrAnalyzer are shown.

This laboratory activity demonstrates that in the case of in-air tests, the 3D models obtained are geometrically and chromatically faithful to the real objects, while in the case of in-water tests, information is partially lost due to the strong refraction effects.

6.1.1 Case study: Terrestrial Application

In the ideal condition of terrestrial scan, the RGB-ITR allows high quality of data, permitting to observe accurate details of all the three sample. The post-processing can provide both colour and structural information at the same time, performing also the colour calibration.

An example of data analysis with ItrAnalyzer is shown in the following figures. It is possible to select a row of the matrix representing the three back-reflection laser layers and the software will show the reflectivity of every single pixel. By selecting a row of the colour corrected images, it is shown the normalized intensity value as a function of the distance (Figure 24).

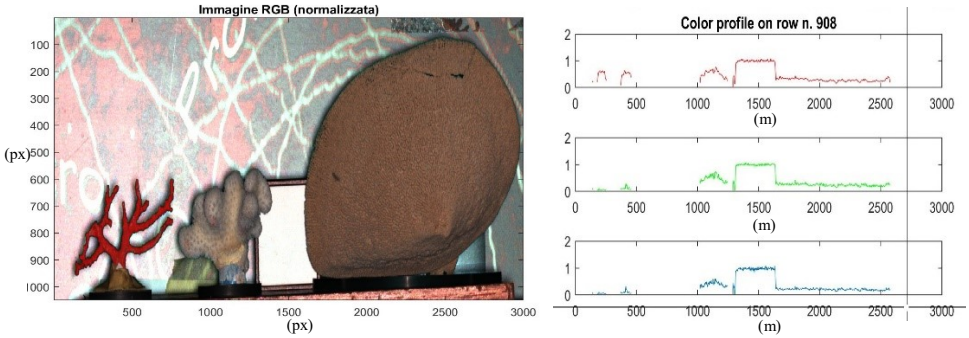

Figure 24 An example of colour profile on a row of the normalized image.

Being the digitization divided into four scans, each processed scan is merged in order to obtain the overall 3D model. In Figure 25, it is shown an example of selected points between two meshes (Figure 25.a) and the related distance errors (Figure 25.b). To optimize mesh

registration and increase the accuracy of the final 3D model, the error between the selected points must be very small.

The final 3D models are modelled by means of an external software, named Meshlab, and results very accurate and detailed (Figure 26). In order to evaluate the performance of the system, the z-profiles of the reconstructed models are selected and plotted (Figure 27). For each model, the depth profile results well defined and has small noise.

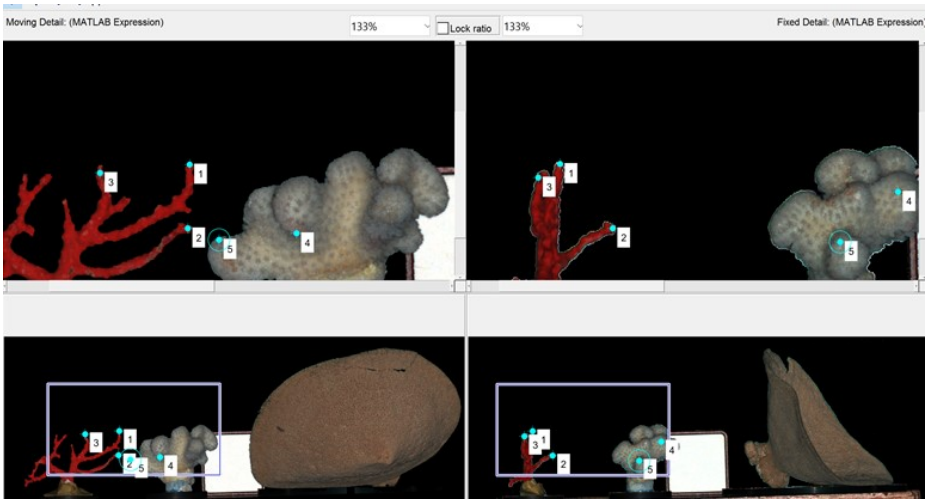

(a)

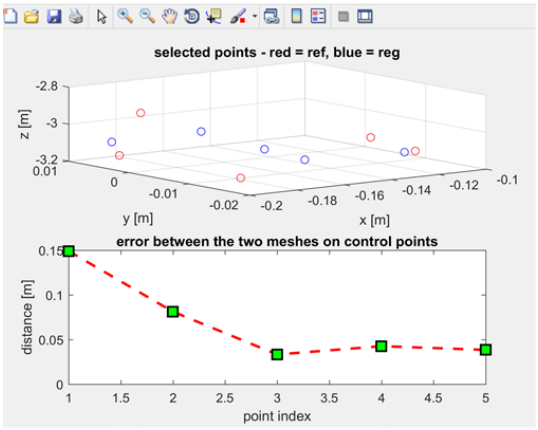

(b)

Figure 25 An example of the manually selection of the reference points between the two meshes (a) and the correspondent distance errors (b).

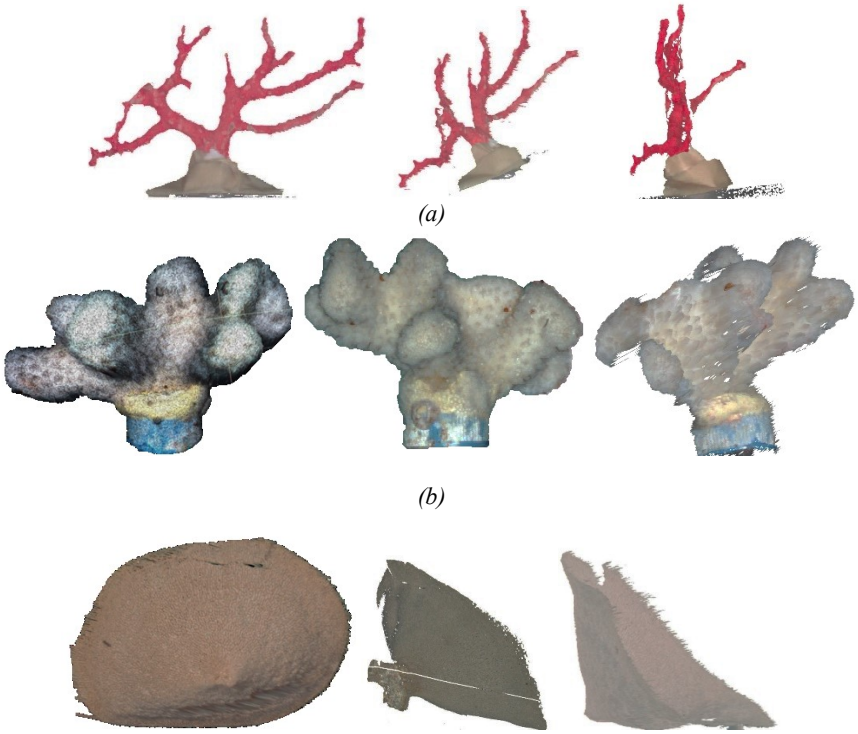

(a)

(b)

(c)

Figure 26 Screen of different configurations of the CR (a), CP (b) and the IC (c) acquired in-air condition.

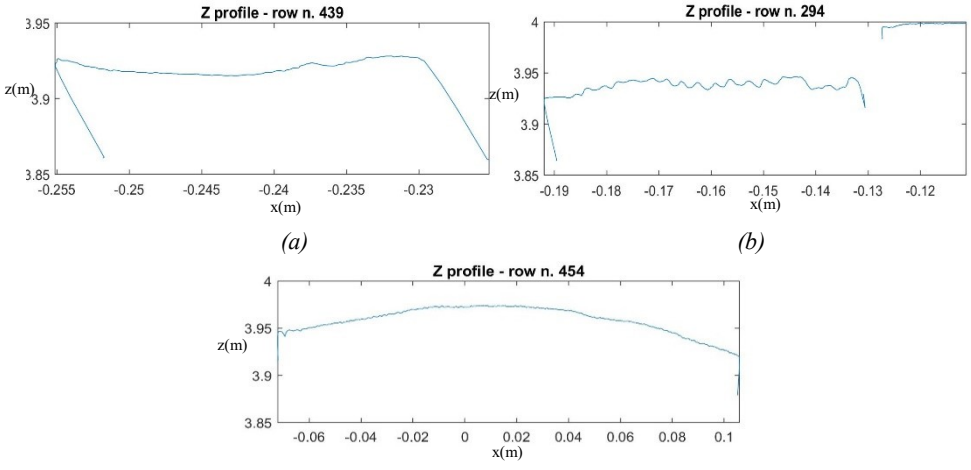

(a)

(b)

(c)

Figure 27 The z-profile of a row of the CR (a), the PC (b) and the IC (c).

6.1.2 Case study: Underwater Application

For what concern the 3D reconstruction by RGB-ITR in in-water condition, it is possible to see the differences between the first and the second model. During the acquisition phase, some external factors difficult to control such as interference due to aquarium glass or to the presence of water, altered the 3D relief. It is possible to see the CR model (Figure 28.a) affected by the high refraction due to both glass and water, and the PC (Figure 28.b) affected only by water refraction. In both cases, the system cannot provide accurate distance and shape information. For this reason, part of the 3D information is lost, due to a noise reduction filter from signal.

Besides, the colour range of the models is not correctly calibrated due to the failure to insert the white target into water. The image normalization is provided by some random points that falsify the colour calibration. However, the three wavelengths are not absorbed by the water as the sample is only a few centimetres deep.

By selecting a row on the 3D models, it is possible to see that the z-profile is affect by higher noise than the previous models acquired in-air (Figure 29). For this reason, it is not possible to evaluate quantitative measurements and assess the level accuracy of these 3D reconstructions.

(a)

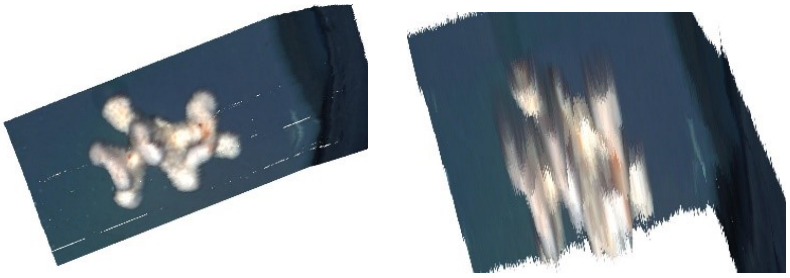

(b)

Figure 28 Screen of different configurations of the CR (a) and the PC (b) acquired in water.

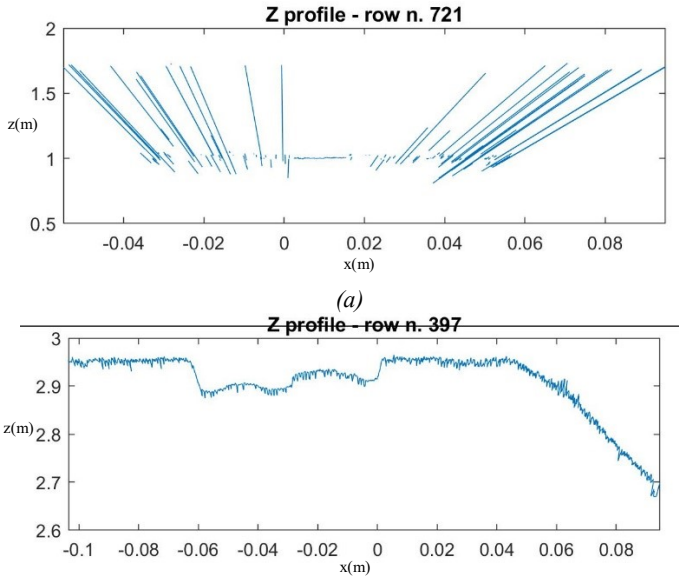

(a)

(b)

Figure 29 The z-profile of one row of the CR (a) and the PC (b) in water condition.

6.2 Colour Correction Algorithm Results

In this Section, results related to the pre-processing of photogrammetric images are presented and discussed. The three phases of the correction procedure, i.e. contrast enhancement, colour restoration, gamma correction, provide enhancement of image quality, very useful in particular for the underwater shooting. The main important role of this algorithm is to improve the recognition of the correspondence points in the Structure from Motion process. Shadows, darkness, colour cast, are all the reasons why the process fail, due to the lack of information.

6.2.1 Contrast Enhancement Results

The image colour enhancement is a simple method that can provide good results; the contrast stretching, operating on each colour channel of small data regions (tiles), allows the analysis of the image portions and computes the appropriate transformations. A limit on the level of contrast enhancement can also be set, thus preventing over-saturation.

In Figure 30, it is shown an example of an enhanced image histogram. It is possible to see that the value distribution of contrast enhanced image covers a wider range then the original image, where the values are clustered to a narrow range (low contrast).

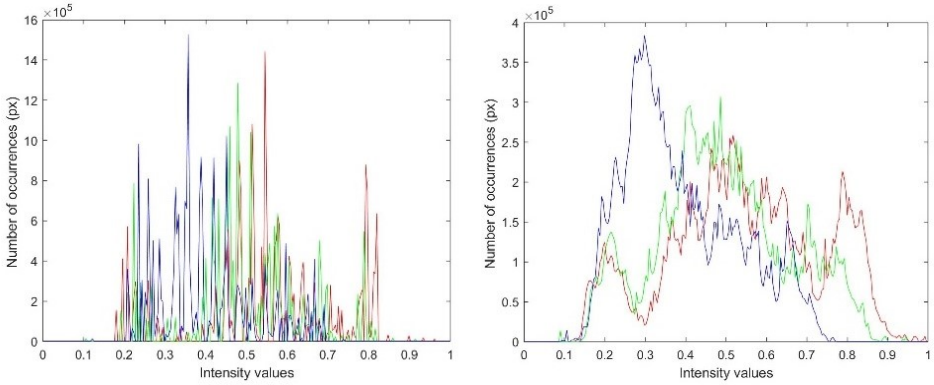

Figure 30 Example of colour enhancement result: on the left there is the original image histogram, on the right there is the stretched colour image histogram.

6.2.2 Colour Balance Results

The second step provides the illuminant estimation of each image, assuming that the average colour patches are grey. Colour balancing of an image alters not only the neutral colours but also the others. The no balanced image is affected by a dominant colour and everything in the image appear with a no correct chromaticity. The colour balance provides to remove the colour cast.

This is shown in Figure 31, where the contrast enhanced histogram of the previous example (on the left) has a dominant blue colour. On the right it is possible to see the balanced colour image, with the three RGB channels climbed by means of the illuminant.

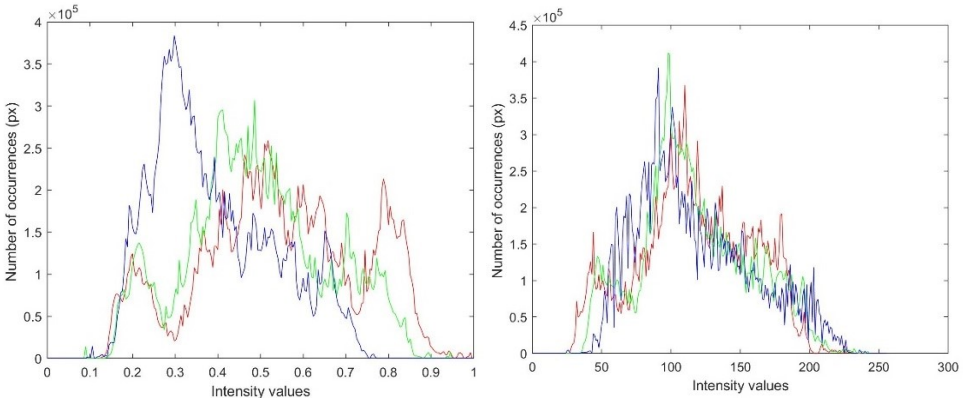

Figure 31 Example of colour balanced result: on the left there is the histogram of the contrast enhanced image, on the right there is the image histogram with grey balance applied.

Figure 32 is an example of the estimated illuminant of two images with different colour balancing, comparing them with the ground truth illuminant. The direction of the estimated illuminant is used for the evaluation of the process. Indeed, the quality of the estimation is evaluated according to the angular error against the ground truth. The smaller the angular error, the better the estimation is. It is highlighted that the ground truth illuminant (red line) is the same for the two corrected images, on the contrary to the estimated illuminant that is different due to the different colour balancing. First image illuminant (yellow line), corresponding to a worst balance with a higher angular error ($\varepsilon_1 = 3.198^{\circ}$) than the second image illuminant (blue line) with a lower angular error ($\varepsilon_2 = 1.672^{\circ}$).

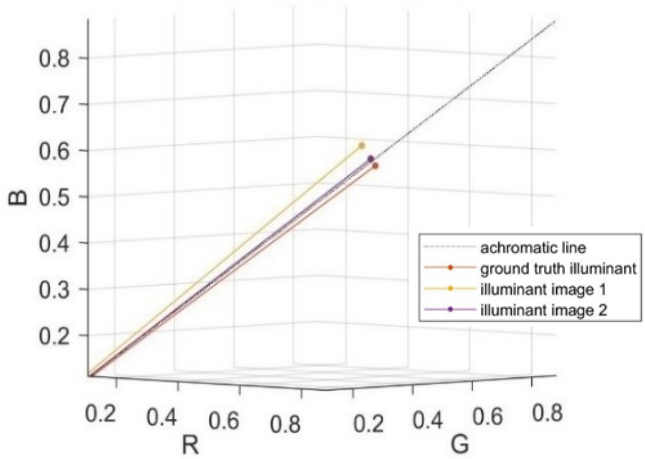

Figure 32 Visualization of the estimated illuminant and the ground trouth of two images with different lighting conditions. Each illuminant represents a vector in RGB space.

6.2.3 Gamma Correction Results

In order to restore also the brightness of the images, the estimated illuminant is used to give the correct illumination of the scene, by means of the gamma correction. The mean of RGB value of the estimated illuminant is the gamma value used for the correction.

By comparing the histogram in Figure 33, obtained from the gamma correction, with the previous histogram, only colour balanced and contrast enhanced, it is possible to see that the image, before the gamma correction has lower intensity values (less than 150). When the gamma value is applied the image intensity is enhanced. The best brightness correction is obtained when the number of occurrence is centred on 150 intensity value.

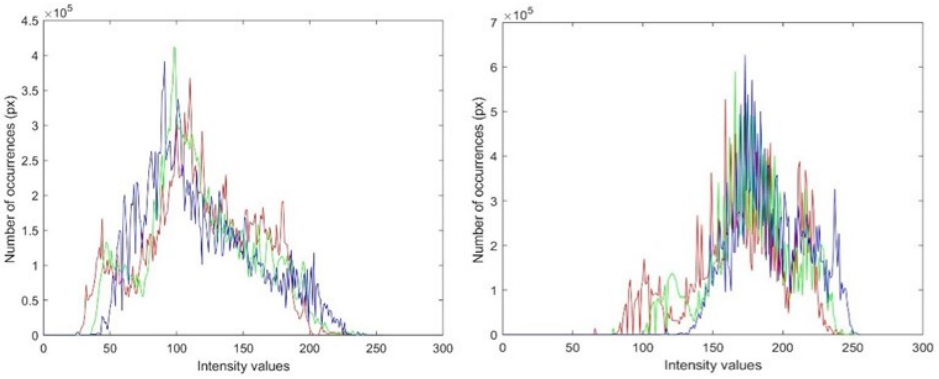

Figure 33 Comparison between the histogram obtained after the colour balancing (on the left) and the histogram of the final colour corrected image (on the right).

The final result is a series of images with colour very similar to those of the object. Figure 34 is an example of the histogram of two restored images by means of the correction procedure. Below, some examples of colour corrected images are shown in-air (Figure 35) and in water condition (Figure 36). All the three Red, Green, and Blue colour channels shows a more even distribution of the pixels intensity.

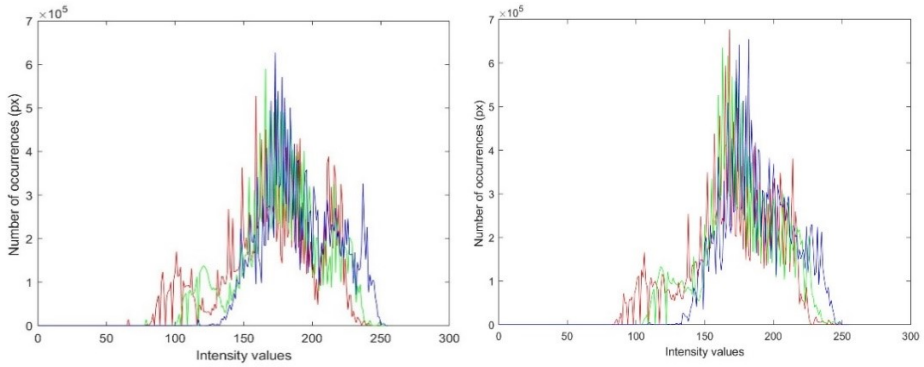

Figure 34 Comparison between the colours corrected histogram of two consecutive images acquired with different lighting conditions.

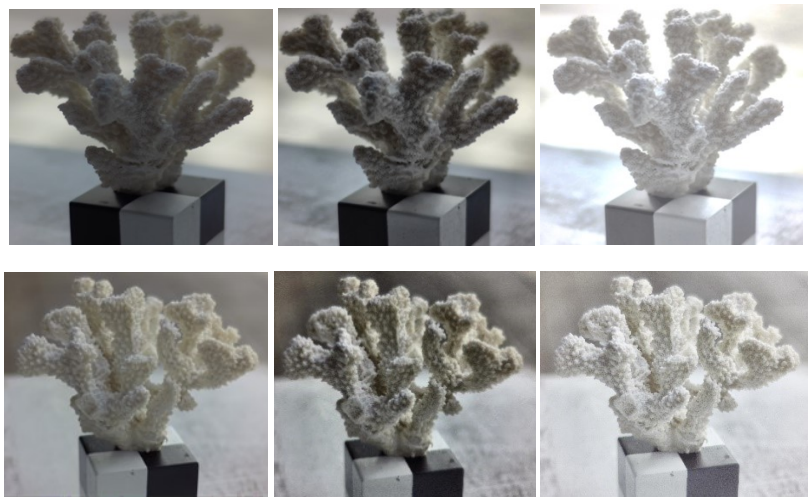

Figure 35 Result of the colour restoration of two images with different lighting conditions: on the left there are the original images, in the centre there are the enhanced images and on the right there are the final corrected colour images.

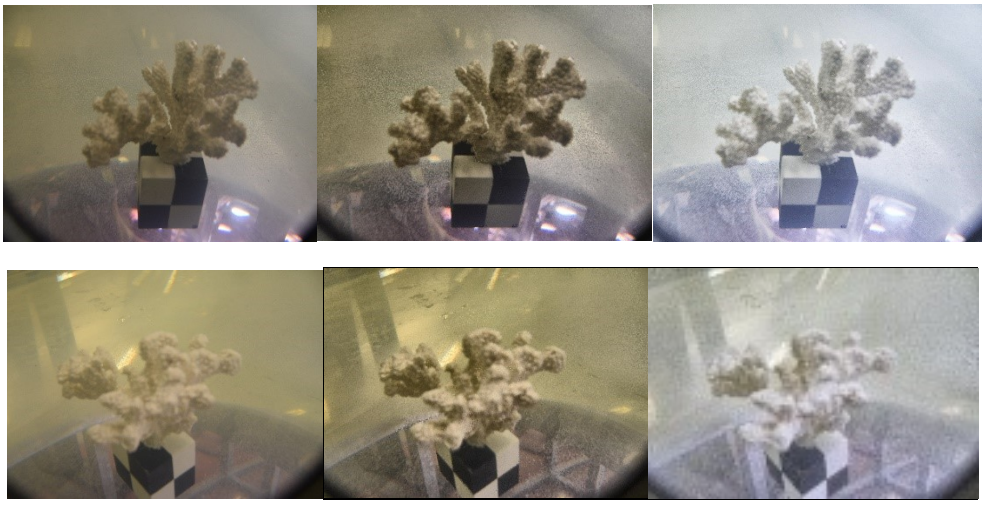

Figure 36 Result of the colour restoration of two underwater images: on the left there are the original images, in the centre there are the enhanced images and on the right there are the final corrected colour image.

6.3 Photogrammetric Results

The optical qualities of camera used in this study are sufficient to produce accurate 3D models of underwater objects. It is demonstrated that the automatic process implemented by Photoscan is able to reconstruct the surfaces and volumes of the 3D sample acquired by means of the three camera lenses. In Table 6, some data from the post-processing phase are summarized.

	Focal length (mm)	**Tie points**	**Flying altitude (cm)**	**Ground resolution (cm/pix)**	**Coverage area (cm^2)**
Dataset 1	16	15070	44.6	0.41	190
	60	37442	161.0	0.45	226
	18-105	17831	55.3	0.46	123
Dataset 2	16	26173	42.5	0.38	200
	60	14115	161.0	0.37	389
	18-105	17686	78.5	0.53	104
Dataset 3	16	2265	30.6	0.40	114
	60	8346	36.8	0.49	206
	18-105	1565	34.6	0.68	131

Table 6 3D data models summarized.

This first evaluation aims to provide the quality assessment of the software. In particular the operability and potentiality of the 3D reconstruction processing of colour corrected images is carried out by examining the geo-referencing procedures on Photoscan. By estimating the positions of the GCPs, the error between the known and calculated values and the relative distances on the 3D models are assessed. This allowed to evaluate the result of the image orientations by means of the SfM process. However, the deviation values strongly depend on the manual selection by the user on the models that introduces random errors.

6.3.1 Case study: Terrestrial Application

The total RMSE associated to the eight points selected on the 3D models, reconstructed from images acquired with the sample in-air, are small for all the used camera lenses (respectively ±0.89 mm for the 16mm lens, ±0.24 mm for the 60mm lens and ±0.51 for with the zoom lens). From these values it is possible to see that the most correct orientation model is the one obtained with the Nikon lens. However, the total RMSE obtained is less than one millimetre for all the camera lenses. These values show that the automatic reconstruction procedures have been successful, providing precise 3D models.

	DATASET 1			
	$RMSE_X$ (mm)	**$RMSE_Y$ (mm)**	**$RMSE_Z$ (mm)**	**$RMSE_{tot}$ (mm)**
Gopro+16mm lens	0.38	0.69	0.40	0.89
Nikon+60mm lens	0.22	0.01	0.08	0.24
Nikon+zoom lens	0.23	0.07	0.45	0.51

Table 7 Total error calculated on the eight reference points for dataset 1.

Some captured screens of the 3D models below, also provide the visual assessment of the reconstructions (Figure 37). All the models acquired in-air condition are accurate and with high details, in particular the one acquired with the 60mm lens.

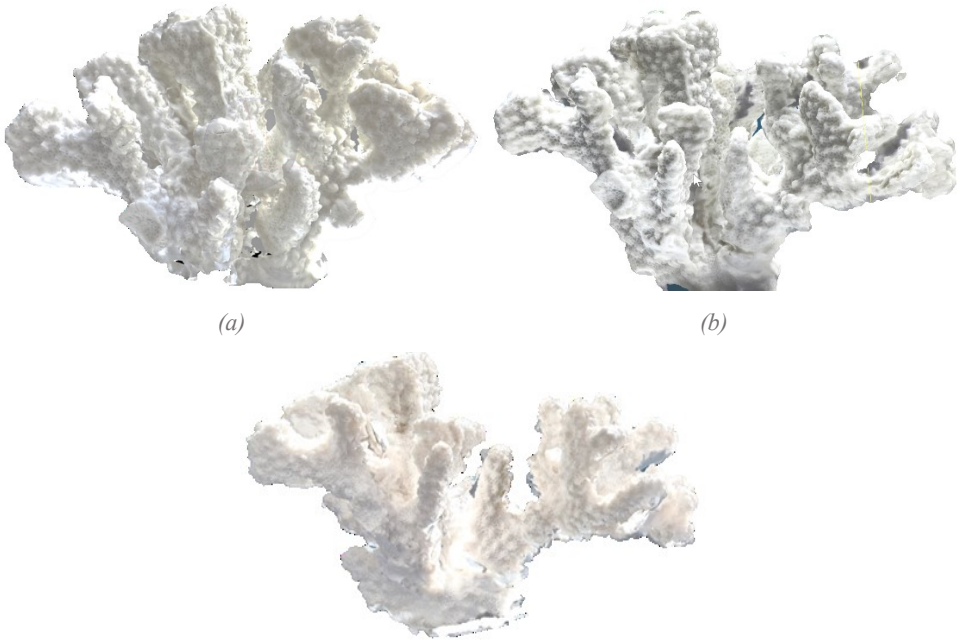

(a) *(b)*

(c)

Figure 37 3D models acquired in-air condition by means of the 16 mm lens (a), the 60 mm lens (b) and the 18-105 mm lens(c).

6.3.2 Case study: Underwater Application

The results related to the acquisition in water are divided in two different datasets, the first one related to the acquisition with the cameras in-air and the sample in water and the second one with both cameras and sample immersed. The difference between the two dataset results are shown below.

6.3.2.1 Dataset: Target immersed in water

The total RMSE associated to the 3D model reconstructed from the sample acquired in-water is higher than the one related to the model reconstructed from images acquired with the sample in-air, in particular for the 60mm camera lens (respectively ±0.90 mm for the 16mm lens, ±2.79 mm for the 60mm lens and ±0.92 for with the zoom lens). This is probably due to some artefacts (e.g. bubbles localised on the sample and on the glass) that the macro lens acquires more than the other two lenses.

	DATASET 2			
	$RMSE_X$ (mm)	**$RMSE_Y$ (mm)**	**$RMSE_Z$ (mm)**	**$RMSE_{tot}$ (mm)**
Gopro+16mm lens	0.74	0.43	0.29	0.90
Gopro+60mm lens	0.60	1.69	2.22	2.79
Nikon+zoom lens	0.78	0.06	0.49	0.92

Table 8 Total error calculated on the eight reference points for dataset 2.

Also from the captured screens of the 3D models below, it is possible to see that all the models have poorly details compared to the previous ones, probably due to the refraction of the aquarium glass and the loss of sharpness due to the bubbles that appear in the shooting.

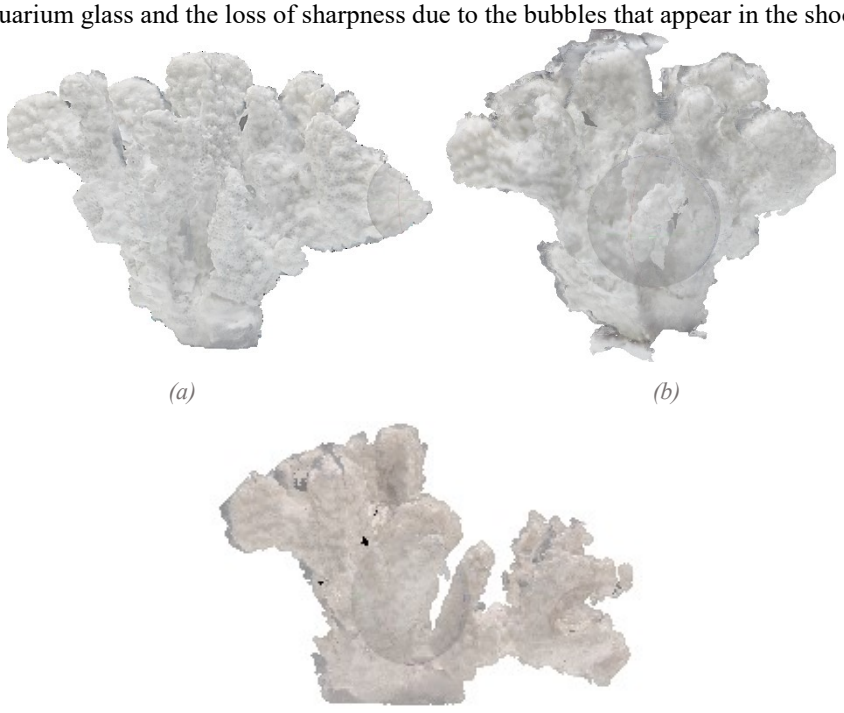

(a) *(b)*

(c)

Figure 38 3D models obtained from dataset 2 by means of the 16 mm lens (a), the 60 mm lens (b) and the 18-105 mm lens(c).

6.3.2.2 Dataset: Target and camera immersed in water

The total RMSE associated to the 3D model reconstructed from the *dataset 3* is not very higher, in particular for the zoom lens (respectively ±1.08 mm for the 16mm lens, ±2.92 mm for the 60mm lens and ±0.92 for with the zoom lens).

	DATASET 3			
	$RMSE_X$ (mm)	**$RMSE_Y$ (mm)**	**$RMSE_Z$ (mm)**	**$RMSE_{tot}$ (mm)**
Gopro+16mm lens	0.43	0.12	0.98	1.08
Nikon+90mm lens	0.01	1.42	2.56	2.92
Nikon+zoom lens	0.74	0.08	0.89	0.92

Table 9 Total error calculated on the eight reference points for dataset 3.

The 3D models are better defined respect to the previous models from *dataset 2*. The reconstructions are geometrically loyal to the real coral and more details are visible.

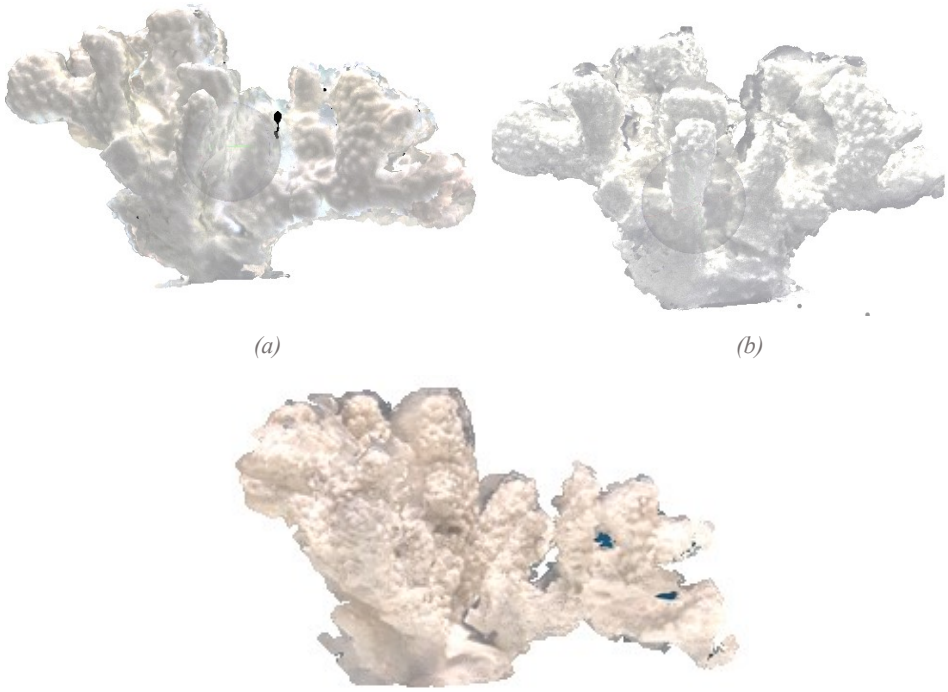

(a) *(b)*

(c)

Figure 39 3D models obtained from dataset 2 by means of the 16 mm lens (a), the 60 mm lens (b) and the 18-105 mm lens(c).

The scaling verification of the models obtained by Photoscan is performed by measuring the relative distances between the GCPs on the models and comparing them with the values measured by means of the digital calibre. Figure 40, Figure 41 and Figure 42 are refer to the results obtained by means of the three camera lenses in the three datasets.

For all the lenses, the error associated to the distance values estimated from the 3D model from *dataset #1* are very small. Precisely, the standard deviation for the 16mm lens is ± 0.7 mm, while for 60mm lens is ± 0.9 mm and for the zoom lens is ± 0.7 mm. On the contrary, the standard deviation is little higher for the other two datasets. In particular, the standard deviation of the estimated distances related to the *dataset #2* is, respectively, ± 1.0 mm for the 16mm lens, ± 2.7 mm for the 60mm and ± 1.1 mm for the zoom lens. Finally, in *dataset #3* the standard deviation is respectively ± 1.6 mm for 16mm, ± 1.01 mm for 60mm lens and ± 1.2 mm for zoom lens. However, all the verified distances indicating no scaling problems.

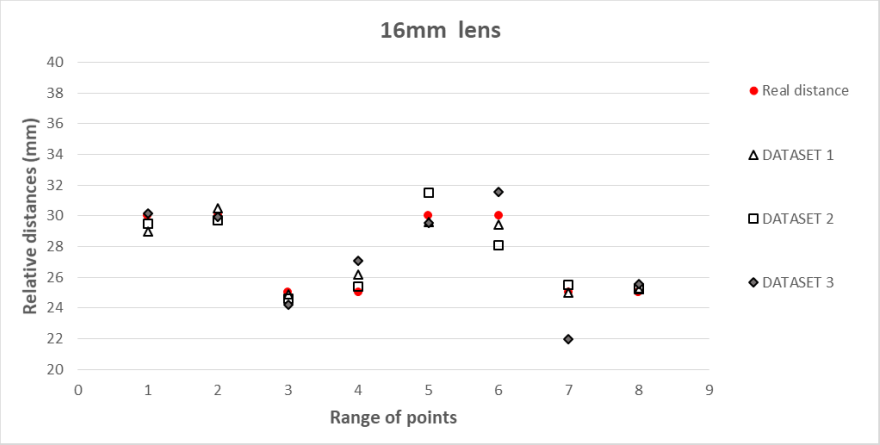

Figure 40 Estimated distances on the 3D models obtained by means of the 16mm lens.

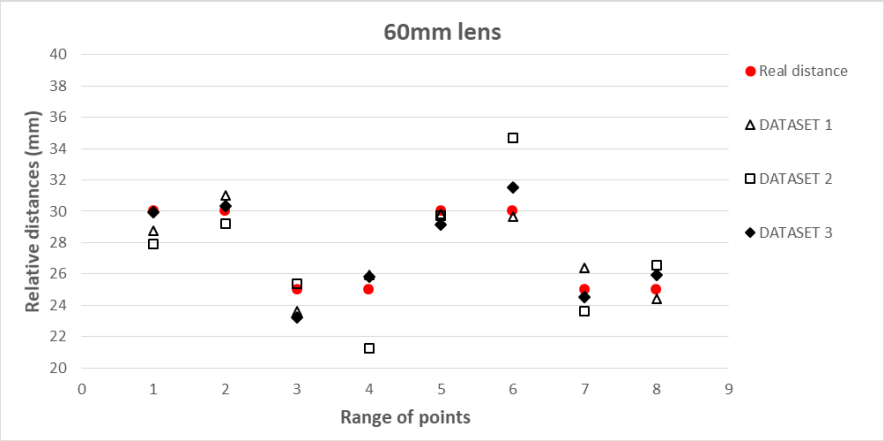

Figure 41 Estimated distances on the 3D models obtained by means of the 60mm lens.

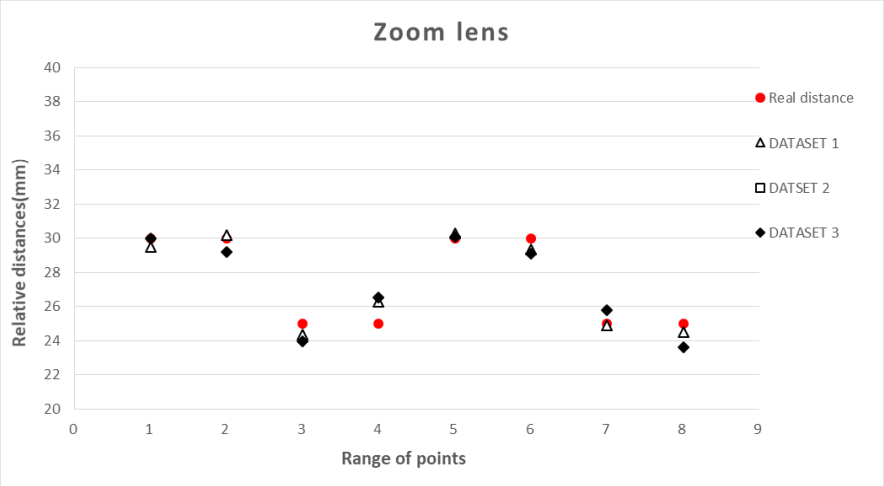

Figure 42 Estimated distances on the 3D models obtained by means of the zoom lens.

7. Quantitative Assessment for Photogrammetric Colour and Shape Reconstruction

This Chapter discusses the accuracy of the colour and shape reconstruction process described in the previous chapters.

In particular, the performances of the colour correction algorithm are obtained by comparing the colour information of corrected images with dedicated spectrophotometry tests, used as references, for both the case study (terrestrial and underwater application). Finally, the main differences between the unprocessed images and the colour restoration level obtained by both the method proposed in [91] and the approach presented in Chapter 4.2, are highlighted.

Moreover, in order to evaluate the precision and accuracy of the reconstructed models, the differences between the dimensional measures of a reference target scanned by a laser displacement sensor and by the photogrammetric technique using the different cameras, are performed.

7.1 Colour Validation

The validation of colour correction algorithm aims to provide the measure uncertainty of the restored images under different lighting conditions, by using the spectrophotometer as gold standard, that is the most precise and accurate colorimetric measurement instrument.

These measurements are performed on 9 tiles with different colour information (Figure 43), acquired before with the spectrophotometer and then compared with the processed images, acquired by the different cameras in-air and then in water condition. The CIE colour system used for the quantitative measurements is the L*a*b* colour space and the colour analysis with the spectrophotometer is performed by using the CIE D65 illuminant and 10 Standard Observer, according to EN ISO 10545-16. On the other hand, the image acquisition uses a white reference tile calibrated with the gold standard instrument. This is because the standard illuminant D65 can be damaged if immersed in water.

The colour matching of tiles acquired by images and spectrophotometer is determined by the colour difference, which defines the chromatic accuracy, described by the following expression (18):

$$\Delta E = \sqrt{\Delta L^{*2} + \Delta a^{*2} + \Delta b^{*2}} \tag{18}$$

where L* is the lightness and a* and b* are the green–red and blue–yellow colour components. The measurements variability within and between the methods is determined by means of the Mean of the Colour Difference from the Mean (MCDM) [105] between repeated measurements, as defined in Eq. 19:

$$MCDM = \frac{\sum_{i=1}^{n} \Delta E_i}{n} \tag{19}$$

where: n is the is the total number of repeat measurement taken in each tile, and the standard deviation of each and overall tiles (ASTM E2214-08, 2008) [106]. The efficiency of the method is evaluated by the percentage of total ΔE reduction compared to the unprocessed images.

7.1.1 Spectrophotometer Colour as Gold Standard

For the evaluation of colour difference, the UV–visible-NIR spectrophotometer, model V670 from Jasco Co., is used in order to determine the colorimetric values of the 9 reference tiles. Before conducting the measure of the tiles, the instrument is calibrated with the white standard target (D65 illuminant), to give a correct sample spectrum. This calibration procedure is replicated for the dark absorbance measure. After calibration, the L*a*b* values of each tile is taken by three measurements and the colour difference is calculated, defining the average and the standard deviation (σ) for all the tiles (Table 10). In this way, it is possible to define the precision of the instrument. From these values, it is possible to see that the instrument has high accuracy for each tile.

Figure 43 The 9 reference tiles used for the colour validation procedure and the whit target (D65 illuminant) in the centre.

Tiles	ΔE_1	ΔE_2	ΔE_3	***MCDM***	σ
Pink	1.22	1.29	0.07	0.86	0.68
Grey	0.88	1.37	0.79	1.01	0.25
Light blue	1.73	1.04	0.70	1.16	0.53
Brown	1.32	1.29	0.19	0.94	0.65
Red	1.38	1.40	0.17	0.98	0.70
Yellow	1.67	1.79	0.18	1.21	0.89
Blue	0.77	0.57	0.40	0.58	0.19
Black	1.39	1.39	0.01	0.93	0.79
Green	0.58	0.33	0.56	0.49	0.14
MCDM	1.22	1.16	0.34	**0.91**	
Σ	0.40	0.45	0.28	0.24	

Table 10 Colour difference measured by spectrophotometer for 9 tiles

7.1.2 Image Colour Correction Accuracy

The mean L*a*b* coordinates of each tile measured by spectrophotometer is used as reference values for the estimation of the performance of the proposed approach, aiming to restore the colour images. The ΔE of each tile is estimated on unprocessed images and then, on the corrected images by means of the colour correction algorithm. A very important aspect of this evaluation is that all tiles are simultaneously acquired. Moreover, three different images with different lighting illumination and both in-air and in water condition were obtained. So, it is possible to evaluate how much colour difference is reduced after the colour correction.

The MCDM and standard deviation of ΔE is calculated for each tile, in order to evaluate the repeatability of the proposed algorithm on the individual colour source. The results are compared with the unprocessed images and the other approach for colour correction proposed by Tan [91].

Figure 44 shows the colour variability of each tile acquired in-air condition. From the results, it is possible to see that the proposed method has lower MCDM values (mean ΔE 7.14) than the other method (mean ΔE 11.47) that means higher inter-repeatability. The highest variability is found for the brown, while in the other methods are found mainly for brown, light blue and grey.

In Table 11, it is possible to see the contribution of each colour to the total ΔE reduction of unprocessed images, for both the methods. The proposed method reduces by 30.80 % of total ΔE of the unprocessed images, except for the brown that is slightly reduces and the green that is increased. On the contrary, the total ΔE obtained by the other method increases of 11.01 %, in particular due to the increase of the colour difference of grey, light blue, yellow and green.

	Method by Tan			***Proposed method***		
Tiles	*MCDM*	*σ*	*ΔE reduction (%)*	*MCDM*	*σ*	*ΔE reduction (%)*
Pink	7.05	3.43	-2.83	8.07	1.84	-1.74
Grey	12.40	4.07	7.46	2.82	0.28	-2.85
Light blue	12.20	5.61	6.87	2.97	0.92	-3.05
Brown	12.54	4.50	-2.42	14.75	6.70	-0.03
Red	13.93	3.18	-0.86	9.48	0.71	-5.64
Yellow	11.94	0.51	0.73	7.15	1.27	-4.42
Blue	14.08	2.23	-1.12	6.69	2.32	-9.07
Black	10.79	1.44	-0.67	7.09	3.33	-4.65
Green	8.26	0.14	3.84	5.26	1.16	0.62

Table 11 Summarized results for each tile in images acquired in-air.

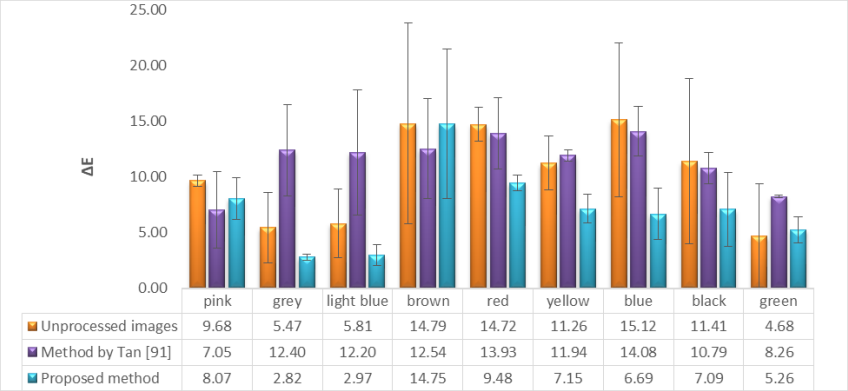

Figure 44 MCDM and standard deviation of images acquired in-air condition.

The results related to the tiles colour measured in underwater images, are shown in Figure 45 and summarized in Table 12. The mean ΔE is lower for proposed method than the method proposed by Tan (mean ΔE 7.54 and mean ΔE 10.35, respectively). Besides, both the methods show higher mean ΔE for red and yellow tiles. This is likely due to the low water absorption level occurring in shallow water. So, it is necessary to underline the utility of the colour compensation only to restore underwater images acquired in very low depth. However, it can be also combined with the artificial lights to optimize the images restoration at greater depths. Finally, from the comparison of the results with the unprocessed images, it is possible to see that both methods reduces the colour difference of tiles compared to the unprocessed images. But also in this case, the colour processed by the proposed method has greater performance in terms of reduction of total ΔE (40.04 % lower) than the other method (11.02 % lower).

	Traditional method			***Proposed method***		
Tiles	*MCDM*	*σ*	*ΔE reduction (%)*	*MCDM*	*σ*	*ΔE reduction (%)*
Pink	11.52	0.79	1.07	8.72	0.66	-1.40
Grey	7.00	3.65	-2.53	4.49	4.82	-4.74
Light blue	5.78	2.72	-4.84	6.13	4.04	-4.53
Brown	6.64	0.05	0.35	7.07	2.03	0.73
Red	17.62	6.33	-0.97	16.54	3.71	-1.93
Yellow	13.94	5.37	-2.87	11.40	3.75	-5.12
Blue	6.41	2.79	-3.84	4.12	2.47	-5.85
Black	12.98	4.40	2.50	5.24	3.89	-4.34
Green	11.24	7.15	-6.62	4.17	6.50	-12.86

Table 12 Summarized results for each tile in underwater images

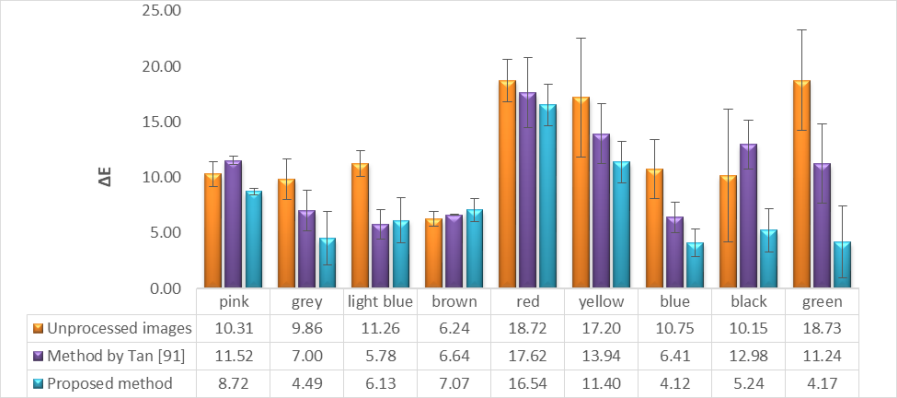

	pink	grey	light blue	brown	red	yellow	blue	black	green
Unprocessed images	10.31	9.86	11.26	6.24	18.72	17.20	10.75	10.15	18.73
Method by Tan [91]	11.52	7.00	5.78	6.64	17.62	13.94	6.41	12.98	11.24
Proposed method	8.72	4.49	6.13	7.07	16.54	11.40	4.12	5.24	4.17

Figure 45 Mean and standard deviation of colour difference of underwater images.

7.2 3D Shape Validation

In this Section, the shape validation of the 3D models acquired by the photogrammetric technique discussed in the work is described. The differences between the different cameras lenses used, in terms of accuracy, are shown hereafter. The validation phase is based on the standard measurements provided by a Laser Displacement Sensor that estimates the z-profile of a reference sample. The sample used for the calibration process, built with known characteristics specifically for this study, is characterized by different steps with fixed height, ranging from 0.5 mm to 2 cm. The quantitative assessment of the reconstructions is characterized by measuring a set of points on the z-profile of the model (10 points for each step) and the measure of four distances at different heights. The uncertainty measurements of each step are provided for all the camera lenses used in this work, both in-air and in water condition.

7.2.1 Laser Displacement Sensor as Gold Standard

For the comparison of vertical profiles, the CCD Laser Displacement Sensor LK-series, from Keyence, is used in order to determine the distances values of the different steps of the know-sized sample. The mean values obtained for each distance are the reference measures for the assessment of the photogrammetric accuracy.

Two different optical heads with different resolution in z are used, the first one with the wider field (measurement range: ±20 mm) to measure the steps in the order of centimetre (respectively 10 mm and 20 mm heights) and the second one with a narrow field (measurement range: ±1.5 mm) to measure the steps in the order of millimetre (respectively 1mm and 0.5 mm heights). Due to these different range, the offset is retrieved to measure the two distances at 10 mm and 20 mm. The mean and the standard deviation (σ) of the measured points for each step, provides the performance of the instrument. In table 13 the results related to the gold standard measurements for each distance are shown. As expected, the instrument has higher precision in the operating range of the two optical heads, slightly reduced when

the measure is near to the out of range. However, the instrument offers high measure precision of each step of the 3D reference sample.

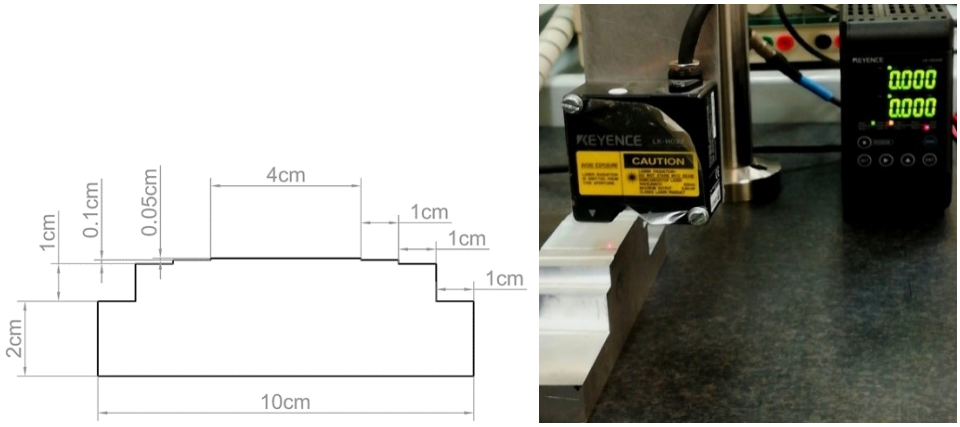

Figure 46 Sample specifications (on the left) and the set up measurement for determination of reference points (on the right).

Distance	***Mean (mm)***	***σ (mm)***
D_0	0.000	0.002
D_1	0.518	0.003
D_2	1.531	0.028
D_3	10.174	0.003
D_4	19.982	0.010

Table 13 Measurements results of the laser displacement sensor

7.2.2 3D Reconstruction Accuracy

The average of each step measured by the gold standard, is used as reference for the assessment of the 3D reconstruction accuracy with the camera lenses. The mean and standard deviation of each distance, measured for all the camera lenses, is calculated in order to evaluate the accuracy on individual step. Figure 47 shows the z-profile described by the point measured on the 3D surface reconstructions in-air condition, and data are summarized in Table 14. From these values it is possible to see that the z-profile obtained by the zoom lens has higher deviation values in the smallest distances, in particular in D_1 and D_2, which can be considered as a low capacity to reconstruct small details of size ≤ 1.5 mm. On the contrary, the other two lenses provide higher deviation values in the greater distances D_3 and D_4. In particular, the 60 mm lens has higher elevation in D_4, while the 16 mm lens has the lowest elevation in D_3 and D_4.

Generally, the z-profile is satisfying for all the reliefs with the standard deviation included in the order of the millimetres in D_3 and D_4 and in the order less than 1 millimetre in D_1 and D_2, except for the zoom lens. However, from the regression analysis with the reference data,

the zoom lens provides the highest correlation (R^2=0.99 mm) compared to the 16 mm (R^2=0.98) and the 60 mm lenses (R^2=0.97).

	Zoom lens		***16 mm lens***		***60 mm lens***	
Distance	*Mean (mm)*	*σ (mm)*	*Mean (mm)*	*σ (mm)*	*Mean (mm)*	*σ (mm)*
D_0	0.00	0.04	0.00	0.36	0.00	0.24
D_1	0.38	0.19	0.54	0.15	0.49	0.13
D_2	0.55	1.06	1.63	0.22	1.17	0.46
D_3	8.51	1.76	7.31	3.03	8.01	2.30
D_4	18.46	1.63	17.87	2.25	22.17	2.50

Table 14 Summary results obtained for the sample acquired in-air condition.

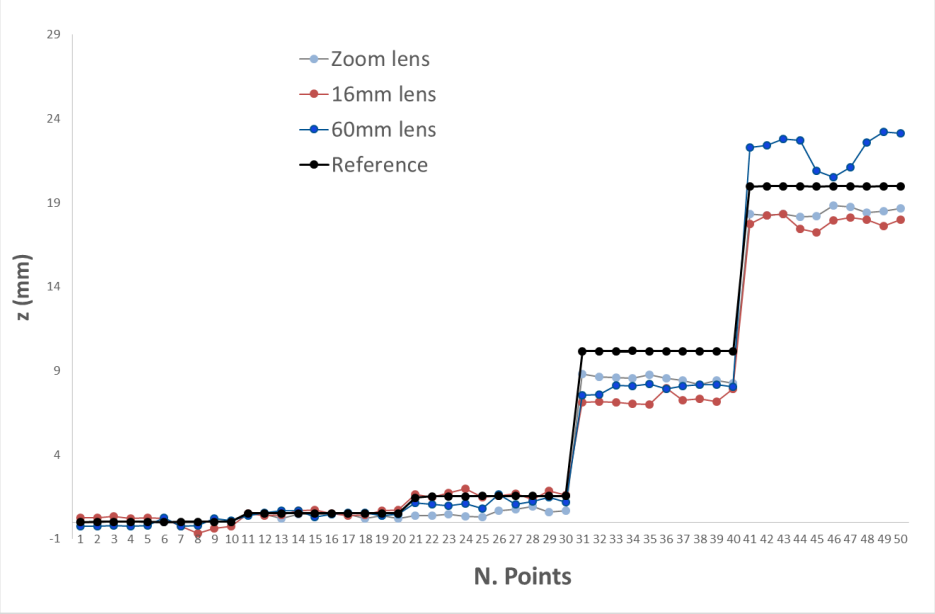

Figure 47 Comparison of the points measured on the z-profiles of the models obtained with different camera lenses in-air condition and the reference points.

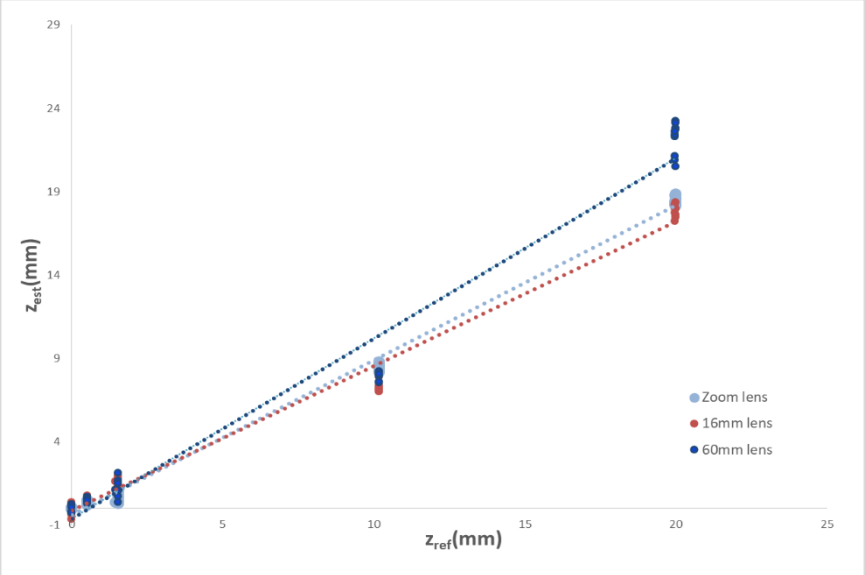

Figure 48 Correlation between the reference and estimated data.

Comparing the z-profiles related to the shape acquired in water, it is possible to see that the 60 mm lens has the best results with the lowest standard deviation in all the measured steps, respectively shorter distances (D_1, D_2) included in the order less than 1 millimetre and larger distances (D_3, D_4) in the order of the millimetre. On the contrary, the zoom and the 16 mm lenses does not provide high accuracy in D_1 and D_2. In addition, for 16 mm lens, also in the other two distances the standard deviation is higher, in particular in D_4, where the standard deviation reaches the order of centimetres. Indeed, from Figure 49, it is possible to see that the 16 mm lens overestimates the two distances. This is probably due to the refraction effect caused by the flat port. Otherwise, the zoom lens underestimates the elevation model, but the standard deviation is included in the order of millimetres.

	Zoom lens		***16 mm lens***		***90 mm lens***	
Distance	*Mean (mm)*	*σ (mm)*	*Mean (mm)*	*σ (mm)*	*Mean (mm)*	*σ (mm)*
D_0	0.00	0.15	0.00	0.37	0.00	0.22
D_1	0.09	0.60	1.23	0.89	0.50	0.07
D_2	0.89	0.88	1.01	0.69	1.66	0.18
D_3	8.16	2.26	14.12	4.19	8.50	1.77
D_4	13.25	7.13	31.52	12.22	19.93	1.18

Table 15 Summary results obtained for the sample acquired in water condition.

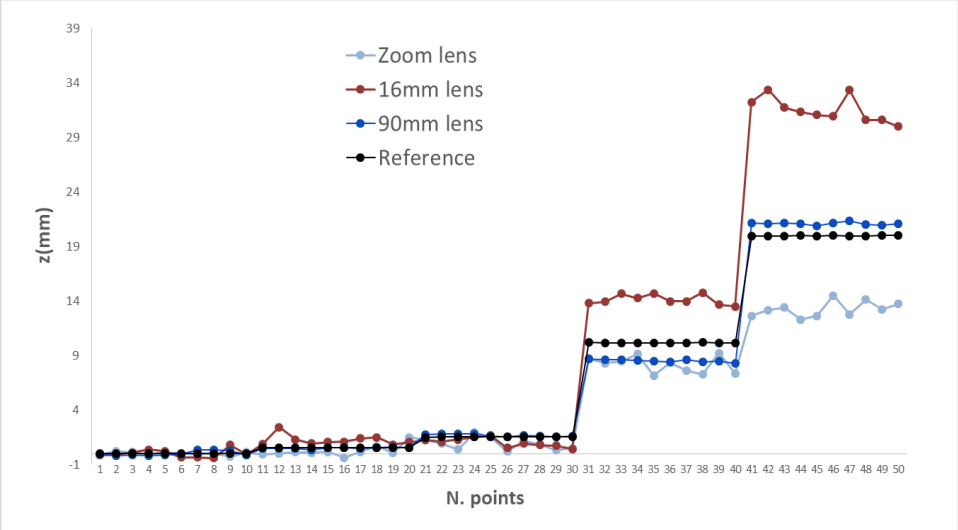

Figure 49 Comparison of the points measured on the z-profiles of the models obtained with different camera lenses in water condition and the reference points.

From data correlation with the reference measures, the 16 mm lens provides the highest correlation coefficient (R^2=0.99) compared to the 90 mm (R^2=0.98) and the zoom mm lenses (R^2=0.91).

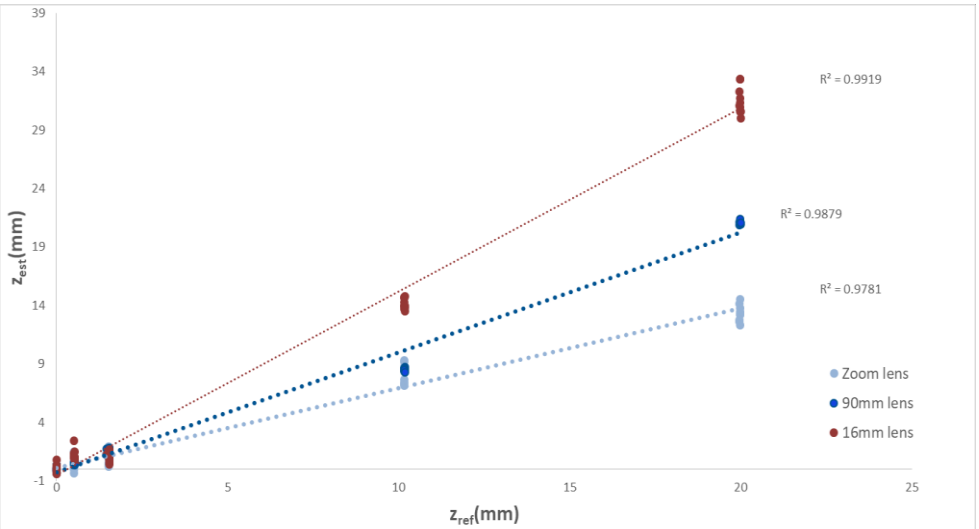

Figure 50 Correlation between the reference and estimated data in water condition.

8. Conclusions

The research carried out within this thesis aimed to identify the best non-contact scanning technique to obtain virtual reconstructions and 3D digital models of real corals in shallow water. The possibility to reproduce the colour and the complex structures of these benthic organisms is a valuable contribution for marine scientists studying coral reefs. However, the focus on isolated corals in shallow water might represent a further issues to standard optical-based approach, since artificial light, which is commonly adopted in underwater applications, might not be exploitable. Indeed, in some cases, the experimenter might be in a testing condition in which the system could lie both outside and inside water.

In particular, the application in subsea environment of two different solutions, the laser-based and the image-based techniques, is analysed and supported by different case study, mainly characterized by in-air and in water acquisitions. The small-sized objects was appropriately selected for size and structural features. Operations, process reliability, quality and metric accuracy of the final products were the examined aspects through the acquisition and processing of different datasets.

In addition to the 3D reconstruction, the colour characterization of the models is a very important aspect widespread in this thesis. The aim of this investigation, besides to render the real colour of the objects, useful to examine the colour alteration on the surface of the coral colonies [107], is to restore the degraded underwater images, due to the non-uniform lighting examine the colour alteration on the surface of the coral colonies conditions, the light absorption and the projected shadows or obscured target from external objects.

For what concern the laser based approach, the terrestrial RGB-ITR scanner laser was adopted to investigate its performance for underwater applications. The terrestrial case study aimed to provide the performance of the system in the ideal investigation. According to the results, it is possible to claim that the system provides detailed analysis of the surface with the z-profiles well defined for each investigated objects. In addition, the colour information is not affected by external light noise. On the other hand, the three wavelengths are not transmitted in water as well as in air, in particular the red channel because of low water absorption level in shallow water (i.e. few cm). From the z-profiles of both the reconstructions, it is possible to see that the models are affected by very high noise, in particular the sample of *dataset 1*, also for the high refraction due to the glass. The sample acquired in *dataset 2* has zero resolution and quality of the 3D shape. In addition, the long acquisition time and the high performance cost of the system are drawbacks for the scuba divers. For these reasons, the RGB-ITR was not studied and tested for further considerations.

Therefore, during the last two years project, the research activity focused on the photogrammetric approach and the implementation of a method to improve the quality of images directly collected underwater. The proposed approach is presented and tested on terrestrial and underwater images acquired by different lighting condition. It is demonstrated that the restoration of degraded images, both in-air and in water conditions, provides the increase of quality images and consequently, the improvement of the 3D reconstruction. Without this pre-processing step, the SfM algorithm is not able to extract the significant features and so to reconstruct the models because of the low quality of raw images acquired under different light illumination.

The efficiency of the method is demonstrated by comparing the raw images with the processed ones and validated by means of the spectrophotometer measures. The samples were appropriately chosen based on the colour and the physical properties that last in water. According to the results, it is demonstrated that the proposed method reduces the colour difference of the unprocessed images in air condition by 30.80 %, while in water condition the 40.04 % is reduced. This is probably due because in air condition the main cause of colour uncertainty is the lightness (L* component) and in the acquired images the difference between the scene illumination was much accentuated. Otherwise the method provides a good restoration of the colorcast that is particularly remarkable in the underwater images. Only for brown colour, the method has not good results: in-air condition, the method has low precision and only the 0.03% of colour difference is reduced, while in water condition even increase. In addition, the red and yellow are slightly reduced in underwater images, probably due to a partial loss of colour information since short depths. This can also be seen from the results of the other method, with which it was compared. The comparison shows also the worst performance of the other method than the proposed one, both in-air and in water condition.

The results concerning a first quality assessment of photogrammetric reconstruction are obtained by means of the horizontal/vertical RMSE of the eight GCPs selected on the 3D models. In the terrestrial case study, the geo-referencing procedure precision is satisfactory for all the three models of *dataset 1* obtained by different camera lenses, with total RMSEs in the order less than 1 millimetre. In the underwater case, for *dataset 2* the total RMSE obtained by 60 mm lens is higher than the other two models (in the order of millimetres). A hypothesis of this higher value is that, being a macro lens, it acquires more artefacts localized around the object (e.g. the bubbles), that increase the noise and reduce the performance of the reconstruction. For *dataset 3*, the total RMSE is not particularly different than the *dataset 2* for all the three camera lenses. This shows a lower performance of the reconstruction in underwater condition than the terrestrial. However, all the errors obtained for the two dataset in the second case study are less than ±3 mm and it is possible to say that the 3D models obtained have good metric quality. From the visual assessment, the model obtained by the 60 mm lens has higher details in *dataset 1* and *dataset 3,* than the other two lenses. While, the model in *dataset 2* is not well defined, according to the previously hypothesis of more artefacts in the acquired images. In general, the models obtained in *dataset 3* detain good quality and details for all the three cameras.

The evaluation of the reconstruction accuracy in both the case studies is provided by the comparison of the z-profile of a known-size sample with the gold standard. According to the results, in air condition all the three lenses provides high accuracy of the 3D models for each section, but the zoom lens has a lower resolution (> 1.5 mm) than the 16 mm lens and the 60 mm lens (≤ 0.5 mm). However, the resolution can be increased with the number of images and the shooting distance. From the linear regression analysis, the best correlation between the estimated and reference values is obtained for the zoom lens. In water condition, the best results are obtained by the 90 mm lens, with high resolution (≤ 0.5 mm) and higher accuracy both for shorter and higher distances. On the contrary, the 16 mm lens has the worst accuracy results in the higher distances because overestimates the values. This is probably due to the flat port refraction, which not occur (or occurs in a very small rate) in the case of a dome port. However, from the linear regression the zoom lens values has the lower correlation with the reference ones.

In conclusion, the comparison between the two different scanning methods presented in this thesis allowed to assert that RGB-ITR is currently not able to scan the objects in underwater environment but it is suitable only for terrestrial applications. In addition to the high refraction (in particular of the red wavelength) due to the water, the instrumentation is very bulky and heavy. Finally, the long acquisition times and the high cost of the system are other relevant drawbacks for the scuba divers.

On the other hand, photogrammetry is more appropriate for rapid and low-cost surveys thanks to the low acquisition times and the cheap cost of the device. It is able to perform accurate and detailed reconstructions of small colonies and individual corals. Different levels of details can be achieved ensuring a high resolution depending on the lens used. In the frame of this work, the research of the best optical solution in order to obtain the best accuracy of the 3D models, highlighting the benefits and the drawback, is a main contribution from the literature:

- The common wide-field lenses are more suitable in terms of size and acquisition times, while the resolution is lower and can alter the size measurement due to the refraction of the glass port.
- The macro lenses are the best solution for a detailed analysis of the surface objects at greater distances, but the main issue is to focus on the object to be investigated not to lose the high performance of hyperlocal.
- The zoom lenses is better in terms of practicality and versatility of shooting distances thanks to the possibility to change the focal length and to focus on the object at different distances.

Finally, the implemented algorithm for colour correction is an important tool, able to enhance and adjust the colours and the illumination of acquired images in shallow water. It also allows to better find match points on the images, increasing the accuracy of the 3D reconstruction. A possible future work, could be the automatization of the image enhancement pre-processing in order to build a whole application (e.g. as a web application) managing the automated reconstruction of the 3D model by the SfM approach.

The next step of this research is to directly test the selected method on the field, in coral reef environments. The realized 3D models can be used to analyse the corals structure and growth, in particular in sites subject to perturbing factors. The reproduction by means of the 3D printing techniques, can be also useful for laboratory studies and for educational purpose.

Appendix A: General Concepts of Digital Photography

The digital image is represented by a two-dimensional array, called raster, composed by rows and columns whose elements of finite dimensions, the pixels (picture element), describe the radiometric content of the image according to a continuous function g (i, j), where i and j are spatial variables. In particular, the formation of the digital image is a process that converts a continuous representation (spatial variables) into a discrete one (radiometric values) and it is called 'digitizing'. This process is characterized by two operations, the sampling and the quantization, the first one linked to the geometric resolution and the second one to the radiometric resolution, on which depends the quality of the image.

When the light reflects one or more surfaces, pass through the lens of the camera and reaches the sensor, the heart of the digitizing instrument. The sensor measures the incident light, which is converted as an electrical voltage with proportional intensity. This electric intensity value is transformed by a converter analogue / digital (ADC) in digital number, i.e. in bits information, and characterizes the radiometric resolution (Figure 51).

However, the radiometric resolution represents the ability of a digital sensor to distinguish between grey-scale values while acquiring an image: the greater the bit number, the greater the number of grey-scale values a spectral sensor can distinguish and, therefore, the higher radiometric resolution of a spectral sensor. 1-bit stands for a sensor that knowns only black and white. 2-bits equals 4 grey-scale values and 4-bits 16 values. For coloured images, each pixel is characterized by three RGB channels (red, green and blue) and each channel range from 0 (colourless) to 255 (saturation of colour). So, a coloured image has (23(8-bit)) = 16,777,216 colours.

Camera Sensors

In the current cameras two types of sensors are used to convert a light signal (photons) into electrical charge (electrons) [108]:

- the CCD (Charge-Coupled Device) image sensor;
- the CMOS (Complementary Metal-Oxide Semiconductor) sensor.

Both the sensors are a two-dimensional array. The difference between CCD and CMOS sensors is in the procedure to transform the electric charge into voltage and transfer it from the chip to the camera.

CCD is characterized by two elements: a photodiode (microsensor) and a 'charge transfer region' that transforms photon into the electric charge. The recorded charge is transported across the chip and deposited in the sense amplifiers, which amplify the signal and transfer it to the A/D converter.

CMOS, on the other hand, uses traditional transistor widely used in electronic applications to make most microprocessor.

Because of the manufacturing differences, there are some noticeable differences that influence the performance of a digital camera. In general, it is possible to say that CCD sensors exceed CMOS in terms of image quality, but they need more energy and are slow in

the ‘read in/out’ operations. On the contrary, CMOS sensors acquire images very quickly but with a lower quality than CCD because the charge is amplified for each pixel, so there is less uniformity of the output data.

The main factors that influence the performance of a digital camera and must to be set, in particular in underwater detection, are:

- *Shutter speed* (*exposure time*)*,* that adjusts the amount of light that reaches the sensor and, consequently, determines the exposure and the blur effect.
- *Sampling rate,* that is the physical distance between adjacent cells of the sensor chip. A sensor with a lower sampling rate has a higher sampling density and therefore provides a higher resolution (in terms of pixels). However, a minor step implies a small area of the sensor that are less sensitive to light and more affected to noise.
- *Fill factor,* which refers to the percentage area of a photodiode useful for collecting light. Usually higher fill factors are preferred. A CCD sensor has a 100% fill factor, much higher percentage than the CMOS sensor. In low light conditions, a CMOS sensor requires larger apertures or slightly longer exposure times than a CCD sensor. To overcome this problem, micro-lenses are often used on every single photodiode, which intercept the light, conveying it to the sensitive parts.
- C*hip size,* which can be in a large variety of formats. As already seen, a large chip size is preferable, as each sensor cell is more photosensitive. On the other hand, the larger chips are more expensive to manufacture, so most compact cameras have a very small chip that causes a proportional compaction of the optics.
- *Ground Sampling Distance* (GSD), that effectively determines the geometric resolution of a digital image and represents the real surface area projected on the focal plane and then on the sensor.

  The GSD is given by the following relation:

$$GSD = D \cdot \frac{L}{f} \tag{14}$$

  where: D is the shooting distance, L is the size of the pixel side and f is the focal length.
- A*nalogue gain,* which defines the sensitivity of a camera. It can be controlled in the most recent digital cameras by setting the ISO sensitivity. A high ISO value has a high gain that allows better performance of a camera in low light conditions, when blurred images may be obtained due to long exposure times. However, high ISO settings amplify the noise effect, which is not very appropriate when images need to be processed for metric applications.
- S*ensor noise,* that depends on the temperature. Each sensor is characterized by a certain thermal noise constituted by the continuous presence of current flow that is always present, even when the digital sensor is not exposed to light. It depends on the quality of the sensor and especially on the temperature at which it is located.
- *Digital post processing,* which are a series of operations operates by most camera to improve the image before compression and storage of pixel values.

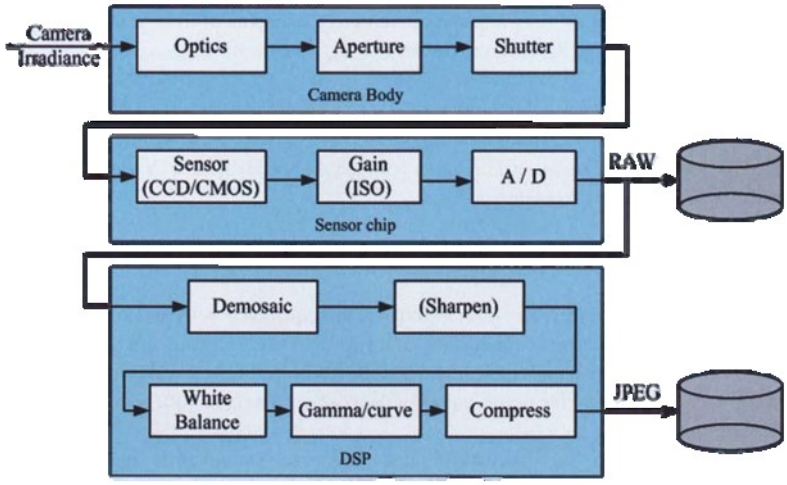

Figure 51 Block diagram of a digital cameras for the formation of the digital image [109].

Types of Camera Lenses

In conjunction with a camera body, different kind of lenses can be used, determining the quality of the images. Indeed, it is very important to adopt the right lens according to the scene or subject to shoot. In the frame of this thesis, not all the lenses could be suitable to provide detailed images of small objects, even more if immersed in water.

The lenses are generally made of dielectric material (transparent to the part of the electro-magnetic spectrum that corresponds to the visible), usually delimited by two spherical surfaces. The spherical lens guarantees a constant angle of refraction and the convergence of light rays in a single plane. They can be subdivided into positive or convergent, i.e. those that deflect on a point of the axis, called fire, all the rays parallel to the axis that cross it, and negative or divergent, which have opposite behaviour.

The fundamental parameters that characterize the classification of the lenses, are shown below.

- *Focal length*: is the primary descriptor of lenses and is defined as the measure (in millimetres) of the distance between the point where light rays converge and the optical centre of the camera lens, while the lens is focused to infinity. A system with a shorter focal length has greater optical power than one with a long focal length. It ranges from just a few millimetres up to over a metre, and can be loosely grouped as in Table 16.
- *Crop factor:* is the ratio of the dimensions of a camera imaging area compared to a reference format (35mm file format, specified as 'full frame', with 36 x 24mm size). It is used to compare the field of view and the image quality of different cameras with the same lens. A higher crop factor correspond to a smaller field of view because a smaller area of the image circle cast by the lens is used by the smaller imaging area. The crop factor is sometimes referred to as 'magnification factor'.

- *Prime or zoom lenses:* a 'prime' lens is one with a fixed focal length, while a 'zoom' lens is one that can zoomed in and out to provide a wider range of focal lengths. Each type has its own benefits and drawbacks. Prime lenses has better optical quality than zooms, and can usually achieve a wider aperture, giving them better low-light performance. Their lack of moving parts also makes them lighter and cheaper. On the other hand, the range of focal lengths offered by a zoom lens can provide more flexibility, making them suitable for a wider range of subjects.
- *Aperture:* the aperture determines how much light it lets through. Often, a wider aperture (lower f-number) is preferable to take photos indoors and when there is little or no natural light. In case of underwater scene with enough natural light (superficial scene acquisition), a closer aperture is recommended in order to reduce the blur.
- *Focusing:* is the point where light rays converge. Physically the focus has a spatial extent, called the 'blur circle'. The non-ideal focusing may be caused by aberrations of the imaging optics. In the absence of significant aberrations, the possible blur circle is smallest the Airy disc, which is caused by diffraction from the optical system aperture. Aberrations tend to get worse as the aperture diameter increases, while the Airy circle is smallest for large apertures. Most modern camera lenses have the autofocus mechanism, while other have the manual system.
- *Image stabilisation:* is used to reduce the blurring, making the shots sharper at slower speeds without using a tripod. The lower the ISO number, the less sensitive it is to the light, while a higher ISO number increases the sensitivity of your camera. This allows better performance in underwater condition.
- *Lens mounts:* allows to attach the lenses to the camera. A lens mount contains mechanical linkages and often also electrical contacts between the lens and camera body. A lens mount may be a screw-threaded type, a bayonet-type, or a breech-lock (friction lock) type. Modern still camera lens mounts are of the bayonet type, because the bayonet mechanism precisely aligns mechanical and electrical features between lens and body.

Focal length	Lens type	Common subjects
8mm-24mm	Ultra-wide angle (fisheye)	Panoramas and skyscapes
24mm-35mm	Wide angle	Interior, architecture, landscapes
35mm-85mm	Standard	General purpose, small objects
85mm-135mm	Short telephoto	Portraits
135mm.300mm	Medium telephoto	Close sports, action
300mm+	Super telephoto	Far sports, wildlife, astronomy

Table 16 Classification of lens focal lengths, types and general uses.

A possible classification of lenses types is shown below:

- **Standard lens**

A standard lens is one with a mid-range focal length, typically around 50mm. They have an angle of view which is roughly the same as the angle that the human eye (about 40°-50°) can comfortably view, meaning that they produce images which appear "natural" to the viewer. Standard camera lenses usually have a fixed focal length and wide aperture, giving them excellent performance in low light. They are popular for a wide range of photography subjects, including landscapes, portraits, and candid shots.

- **Macro lens**

A macro lens is one designed especially for close-up photography. They have a different internal construction from normal lenses which gives them very good sharpness and contrast, meaning that they produce some really eye-catching photos. Macro lenses are useful for photographing any subject at very close range. Typical subjects include insects, animals, and plants, but they are also popular for taking extremely detailed photos of everyday objects.

- **Telephoto lens**

A telephoto lens has a long focal length and provides a high level of magnification, allowing to provide photograph of subjects at a moderate to far distance. They tend to be bigger and heavier than other types of lens, although modern technological advances have made them more compact and easier to handle. Telephoto lenses are popular for any type of photography where you can't get near to the subject, including wildlife and sports events. They are also commonly used in portrait photography, where a moderate telephoto lens will provide a natural, undistorted perspective.

- **Wide-angle lens**

A wide angle lens is one with a short focal length. They provide an angle of view beyond that of a standard lens (from 50° to 180°), allowing them to capture more of the scene in a single shot. Extreme wide angle lenses are known as fisheye lens; these can capture around 180 degrees, making for some intriguing, almost abstract photos. Wide angle lenses are useful for photographing landscapes, cramped interiors, and other subjects which won't fit into a normal lens's field of view. Fisheye lenses take this even further, and are popular for photographing action sports like skateboarding and surfing, where their inherent distortion gives photos a dynamic feel.

Appendix B: PhotoScan Software

Agisoft PhotoScan is a low-cost software package that uses images in order to obtain high quality 3D models. The software is based on a multi-view reconstruction and is efficient also with a large number of images. The SfM algorithm identifies the spatial relationships between the image locations removing gross errors and allowing such visually impressive 3D models to be generated. “Photos can be taken from any position, providing that the object to be reconstructed is visible on at least two photos. Both image alignment and 3D model reconstruction are fully automated” [110] . The procedure of image processing and 3D model reconstruction is schematized in Figure 52.

As mentioned before (paragraph 5.3), several *editing* commands can be used to modify or improve the 3D model obtained, such as the removal of disconnected triangles, the holes filling, etc. The scaling and the geo-referencing procedures of the models can be carried out only after the 3D reconstruction, positioning the GCP points directly on the images.

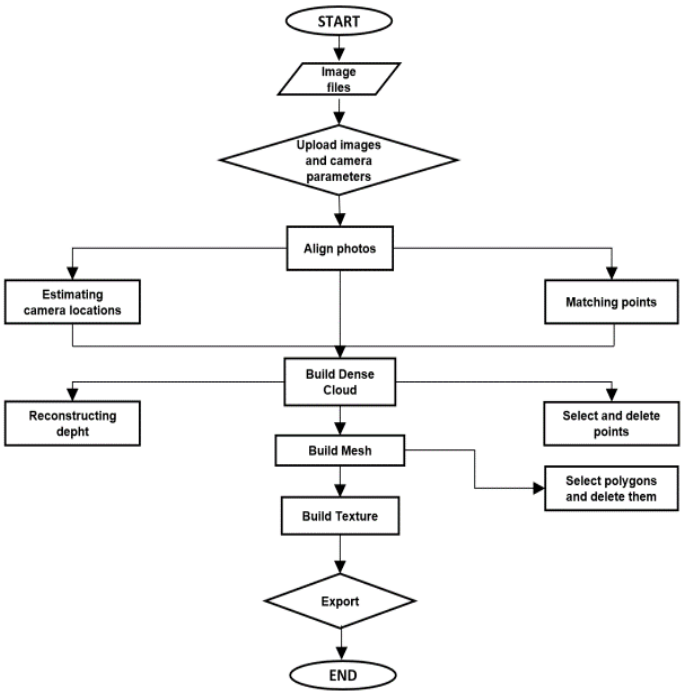

Figure 52 Photogrammetric 3D reconstruction procedure schematized

In Figure 53 it is shown the comparison between the alignment phase applied to the original (a) and corrected images by means of the colour correction procedure (b). In the first case, the misaligned cameras are due to the missing points correspondences on the images because of the low quality and the different scene illumination that cause a high point reproduction

errors. In the second case, it is possible to see that the 3D model is well reconstructed thanks to the colour corrected images.

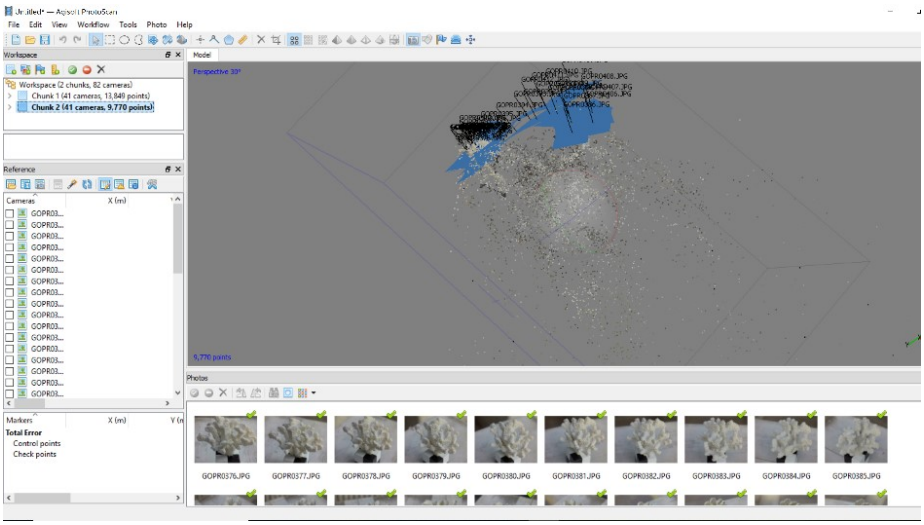

(a)

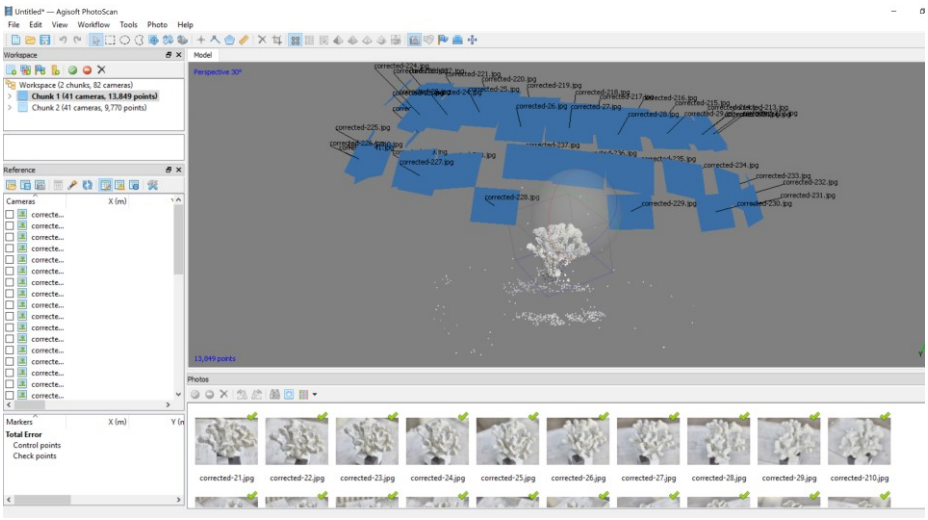

(b)

Figure 53 Comparison between the alignment phase of the original (a) and the corrected images (b)

References

[1] MacIntyre, L. Hugh, Geider, J. Richard, Miller and C. Douglas, "Microphytobenthos: the ecological role of the "secret garden" of unvegetated, shallow-water marine habitats. I. Distribution, abundance and primary production," *Estuaries,* no. 19.2, pp. 186-201, 1996.

[2] G. Bressan, R. Chemello, M. F. Gravina, M. C. Gambi, A. Peirano, S. Cocito and A. Tursi, "Altre principali biocostruzioni," in *Relini G. Biocostruzioni Marine. Elementi di architettura naturale. Ministero dell'Ambiente e della Tutela d Territorio e del Mare*, Museo Friulano di Storia Naturale-Comune di Udine, 2009.

[3] P. Casado-Amezua, G. Gasparini and S. Goffredo, "Phenological and morphological variations in the Mediterranean orange coral Astroides calycularis between two distant localities," *Zoology,* vol. 116, no. 3, pp. 159-167, 2013.

[4] A. Peirano, C. Morri, C. N. Bianchi, J. Aguirre, F. Antonioli, G. Calzetta and P. Orrù, "The Mediterranean coral Cladocora caespitosa: a proxy for past climate fluctuations?," *Global and planetary Change,* vol. 40, no. 1, pp. 195-200, 2004.

[5] M. Dappiano and M. C. Gambi, "New data on occurrence of thermophile Scleractinia (Cnidaria, Anthozoa) in the Phlaegrean Island (Ischia, Procida, Vivara, Gulf of Naples), with special attention to," *Biogeographia,* no. 25, 2004.

[6] "https://www.epa.gov/bioiweb1/aquatic/index.html".

[7] J.-P. Royer and e. al., "Photogrammetric Surveys and Geometric Processes to Analyse and Monitor Red Coral Colonies," *Journal of Marine Science and Engineering,* vol. 6.2, p. 42, 2018.

[8] C. D. Darwin, "The structure and distribution of coral reefs," *Appleton,* vol. 15, 1889.

[9] M. Schwartz, "Encyclopedia of coastal science," *Springer Science & Business Media,* 2006.

[10] A. B. Pittock, "Coral reefs and environmental change: adaptation to what?," *American Zoologist,* Vols. 39(1),, pp. 10-29, 1999.

[11] O. Hoegh-Guldberg and J. F. Bruno, "The impact of climate change on the world's marine ecosystems," *Science,* vol. 328, 2010.

[12] "courses.washington.edu/ocean101/Lex/Lecture23.pdf," [Online].

[13] J. Chappell, "Coral morphology, diversity and reef growth," *Nature Publishing Group,* 1980.

[14] S. Cocito, M. Chiantore, G. Santangelo, G. Bavestrello, C. Cerrano, M. Mistri and V. Zupo, "Monitoraggio delle popolazioni animali naturali," *Biol Mar Medit,* vol. 10, pp. 327-366, 2003.

[15] J. B. C. Jackson, "Morphological strategies of sessile animals.," *Biology and systematic of colonial organisms,,* pp. 499-555, 1979.

[16] J. Chappell, "Coral morphology, diversity and reef growth," *Nature,* vol. 286, 1980.

[17] M. Parry and J. N. C. Committee., “Review of international Marine Protected Area seabed monitoring and assessment of ‘good practice' to inform application within UK waters: a report prepared for JNCC.,” 2012.

[18] N. Yoccoz, J. Nichols and T. Boulinier, “Monitoring of biological diversity in space and time,” *Trends Ecole,* vol. 16, p. 446−453, 2001.

[19] J. M. Lough and N. E. Cantin, “Perspectives on massive coral growth rates in a changing ocean,” *The Biological Bulletin,* vol. 226, 2014.

[20] S. Katsanevakis, A. Weber, C. Pipitone, M. Leopold, M. Cronin, M. Scheidat and I. de Boois, “Monitoring marine populations and communities: methods dealing with imperfect detectability,” *Aquatic Biology,* vol. 16.1, no. 31-52, 2012.

[21] M. Holcomb, A. L. Cohen and D. C. McCorkle, “An evaluation of staining techniques for marking daily growth in scleractinian corals,” *Journal of Experimental Marine Biology and Ecology,* vol. 440, pp. 126-131, 2013.

[22] R. W. Buddemeier, J. E. Maragos and D. W. Knutson, “Radiographic studies of reef coral exoskeletons: rates and patterns of coral growth.,” *Journal of Experimental Marine Biology and Ecology,* vol. 14, pp. 179-199, 1974.

[23] A. Logan and I. H. Anderson, “Skeletal extension growth rate assessment in corals, using CT scan imagery,” *Bulletin of marine science,* vol. 49, pp. 847-850, 1991.

[24] K. Nishida, K. Ishikawa, A. Iguchi, Y. Tanaka, M. Sato, T. Ishimura and A. Suzuki, “Skeletal oxygen and carbon isotope compositions of Acropora coral primary polyps experimentally cultured at different temperatures,” *Geochemistry, Geophysic, Geosystems,* vol. 15, pp. 2840-2849, 2014.

[25] R. J. Lucas, S. N. Peirson, D. M. Berson, T. M. Brown, H. M. Cooper, C. A. Czeisler and L. L. Price, “Measuring and using light in the melanopsin age,” *Trends in neurosciences,* vol. 37.1, pp. 1-9, 2014.

[26] G. Bianco, A. Gallo, F. Bruno and M. Muzzupappa, "A comparative analysis between active and passive techniques for underwater 3D reconstruction of close-range objects," *Sensors,* vol. 13.8, pp. 11007-11031, 2013.

[27] M. Massot-Campos and G. Oliver-Codina, “Optical sensors and methods for underwater 3D reconstruction,” *Sensors,* vol. 15.12, pp. 31525-31557, 2015.

[28] M. Prats, J. J. Fernández and P. J. Sanz, “An approach for semi-autonomous recovery of unknown objects in underwater environments,” *Optimization of Electrical and Electronic Equipment (OPTIM)13th International Conference on,* pp. 1452-1457, 2012.

[29] M. Kulawiak and Z. Łubniewski, “3D imaging of underwater objects using multibeam data,” *Hydroacoustics,* vol. 17, 2014.

[30] Y. Guo, “3D underwater topography rebuilding based on single beam sonar,” *Signal Processing, Communication and Computing (ICSPCC), IEEE International Conference on,* pp. 1-5, 2013.

[31] E. Coiras, Y. Petillot and D. M. Lane, “Multiresolution 3-D reconstruction from side-scan sonar images,” *IEEE Transactions on Image Processing,* vol. 16.2, pp. 382-390, 2007.

[32] K. Pathak, A. Birk and N. Vaskevicius, “Plane-based registration of sonar data for underwater 3D mapping.,” *Intelligent Robots and Systems (IROS), 2010 IEEE/RSJ International Conference on,* pp. 4880-4885, 2010.

[33] N. Hurtós, X. Cufí and J. & Salvi, “Calibration of optical camera coupled to acoustic multibeam for underwater 3D scene reconstruction,” *OCEANS 2010 IEEE-Sydney,* pp. 1-7, 2010.

[34] N. Brahim, D. Guériot, S. Daniel and B. Solaiman, “3D reconstruction of underwater scenes using DIDSON acoustic sonar image sequences through evolutionary algorithms,” *OCEANS, 2011 IEEE-Spain,* pp. 1-6, 2011.

[35] L. J. Mullen, A. J. Vieira, P. R. Herezfeld and V. M. Contarino, “Application of RADAR technology to aerial LIDAR systems for enhancement of shallow underwater target detection,” *IEEE Transactions on microwave theory and techniques,* vol. 43.9, 1995.

[36] B. D. Reineman, L. Lenain, D. Castel and W. K. Melville, “A portable airborne scanning lidar system for ocean and coastal applications. Journal of Atmospheric and oceanic technology,,” *Journal of atmosfpheric and oceanic technology,* vol. 26.12, pp. 2626-2641, 2009.

[37] N. Cadalli, P. J. Shargo, D. C. Munson and A. C. Singer, “Three-dimensional tomographic imaging of ocean mines from real and simulated lidar returns,” *Ocean Optics: Remote Sensing and Underwater Imaging,* vol. 4488, pp. 155-167, 2002.

[38] F. M. Caimi and F. R. Dalgleish, “Performance considerations for continuous-wave and pulsed laser line scan (LLS) imaging systems,” *Journal of the European Optical Society-Rapid publications,* vol. 5, 2010.

[39] D. McLeod, J. Jacobson, M. Hardy and C. Embry, “Autonomous inspection using an underwater 3D LiDAR.,” *Oceans-San Diego, 2013,IEEE,* p. 1.8, 2013.

[40] “Teledyne CDL. INSCAN 3D Scanning Subsea Laser. (accessed on 27 October 2018). Available online: http://teledyne-cdl.com/events/”.

[41] K. H. Thiel and A. Wehr, “Performance capabilities of laser scanners–an overview and measurement principle analysis. International Archives of Photogrammetry,,” *Remote Sensing and Spatial Information Sciences,* vol. 36, pp. 14-18, 2004.

[42] B. Cochenour, L. Mullen and J. Muth, “Modulated pulse laser with pseudorandom coding capabilities for underwater ranging, detection, and imaging.,” *Applied Optics,,* vol. 50.33, pp. 6168-6178, 2011.

[43] L. J. Mullen, V. M. Contarino, A. Laux, B. M. Concannon, J. P. Davis, M. P. Strand and B. W. Coles, “Modulated laser line scanner for enhanced underwater imaging,” *Airborne and In-Water Underwater Imaging,* vol. 3761, pp. 2-10, 1999.

[44] J. Jaffe, “Computer modeling and the design of optimal underwater imaging systems,” *Ocean. Eng.,* vol. 15, pp. 101-111, 1990.

[45] “ 2G Robotics ULS-100 Underwater Laser Scanner for Short Range Scans. [(accessed on 27 October 2018)]. Available online: http://www.2grobotics.com/products/underwater-laser-scanner-uls-100/”.

[46] “2G Robotics ULS-200 Underwater Laser Scanner for Mid Range Scans. [(accessed on 27 October 2018)]. Available online: http://www.2grobotics.com/products/underwater-laser-scanner-uls-200/”.

[47] “2G Robotics ULS-500 Underwater Laser Scanner for Long Range Scans. [(accessed on 27 October 2018))]. Available online: http://www.2grobotics.com/products/underwater-laser-scanner-uls-500/”.

[48] “Savante SLV-50 Laser Vernier Caliper. [(accessed on 27 October 2018)]. Available online: http://www.savante.co.uk/wp-content/uploads/2015/02/Savante-SLV-50.pdf.”.

[49] P. Fechteler, P. Eisert and J. Rurainsky, “Fast and High Resolution 3D Face Scanning,” *ICIP,* vol. 3, pp. 81-84, 2007.

[50] G. S. C. Inglis, I. Vaughn and C. Roman, “A pipeline for structured light bathymetric mapping,” *In Intelligent Robots and Systems (IROS), 2012 IEEE/RSJ International Conference on,* pp. 4425-4432, 2012.

[51] A. Bodenmann, B. Thornton, T. Nakataniy and T. Ura, “3D colour reconstruction of a hydrothermally active area using an underwater robot,” *OCEANS 2011,* pp. 1-6, 2011.

[52] A. Bodenmann, B. Thornton and T. Ura, “Development of long range color imaging for wide area 3D reconstructions of the seafloor,” *Underwater Technology Symposium (UT), 2013 IEEE International,* pp. 1-5.

[53] A. Bodenmann, B. Thornton, R. Nakajima, H. Yamamoto and T. Ura, “Wide area 3D seafloor reconstruction and its application to sea fauna density mapping,” *Oceans-San Diego, 2013,* pp. 1-5, 2013.

[54] S. Tetlow and J. Spours, “Three-dimensional measurement of underwater work sites using structured laser light,” *Measurement Science and Technology,* vol. 10.12, 1999.

[55] “Tritech. Sea Stripe ROV/AUV Laser Line Generator. (accessed on 27 October 2018). Available online: http://www.tritech.co.uk/product/rov-auv-laser-line-generator-seastripe”.

[56] J. Salvi, S. Fernandez, T. Pribanic and X. Llado, “A state of the art in structured light patterns for surface profilometry,” *Pattern recognition,* vol. 43.8, pp. 2666-2680, 2010.

[57] F. Bruno, G. Bianco, M. Muzzupappa, S. Barone, A. V. & Razionale and ., “Experimentation of structured light and stereo vision for underwater 3D reconstruction,” *ISPRS Journal of Photogrammetry and Remote Sensing,* vol. 66.4, pp. 508-518, 2011.

[58] Q. Zhang, Q. Wang, Z. L. Y. Hou and X. Su, “Three-dimensional shape measurement for an underwater object based on two-dimensional grating pattern projection,” *Optics & Laser Technology,* vol. 43.4, pp. 801-805, 2011.

[59] N. Törnblom, “Underwater 3D Surface Scanning Using Structured Light,” 2010.

[60] A. Dancu, M. Fourgeaud, Z. Franjcic and R. Avetisyan, “Underwater reconstruction using depth sensors,” *SIGGRAPH Asia 2014 Technical Briefs,* 2014.

[61] “www.3dnatives.com/en/structured-light-projection-3d-scanning/,” [Online].

[62] A. Bombino, “Valutazione sperimentale di algoritmi di visione stereo finalizzata a una successiva implementazione su FPGA,” *Doctoral dissertation.*

[63] “www.cs.auckland.ac.nz/courses/compsci773s1c/lectures/773-GG/topCS773.htm,” [Online].

[64] M. González-Rivero, P. Bongaerts, O. Beijbom, O. Pizarro, A. Friedman, A. Rodriguez-Ramirez and R. Vevers, “The Catlin Seaview Survey–kilometre-scale seascape assessment, and monitoring of coral reef ecosystems,” *Aquatic Conservation,* 2014.

[65] F. Bonin-Font, A. Cosic, P. L. Negre, M. Solbach and G. Oliver, “Stereo SLAM for robust dense 3D reconstruction of underwater environments,” *OCEANS 2015-Genova,* pp. 1-6, 2015.

[66] J. X. Leon, C. M. Roelfsema, M. I. Saunders and S. R. Phinn, “Measuring coral reef terrain roughness using ‘Structure-from-Motion’close-range photogrammetry.,” *Geomorphology,* vol. 242, pp. 21-28, 2015.

[67] J. Oliensis, “A multi-frame structure-from-motion algorithm under perspective projection,” *International Journal of Computer Vision,* Vols. 34.2-3, pp. 163-192, 1999.

[68] J. Drafahl and S. Drafahl, “Master guide for underwater digital photography,” *Amherst Media,* 2005.

[69] “en.wikipedia.org/wiki/Underwater_photography,” [Online].

[70] M. Guarneri, M. F. de Collibus, G. Fornetti, M. Francucci, M. Nuvoli and R. Ricci, “Remote Colorimetric and Structural Diagnosis by RGB-ITR Color Laser Scanner Prototype,” *Advances in Optical Technologies,* 2012.

[71] L. Bartolini, A. Bordone and A. Coletti, “Laser In vessel viewing system for nuclear fusion reactors,” *High-Resolution Wavefront Control: methods, Devices, and Applications II,* vol. 4124, pp. 201-211, 2000.

[72] De Dominicis L., “Terrestrial and Subsea 3D Laser Scanners for Cultural Heritage Applications,” *Rivista bimestrale ENEA,* 2012.

[73] A. Danielis, M. Guarneri, M. Francucci, M. F. D. Collibus, G. Fornetti and A. Mencattini, “A Quadratic Model with Nonpolynomial Terms for Remote Colorimetric Calibration of 3D Laser Scanner Data Based on Piecewise Cubic Hermite Polynomials,” *Mathematical Problems in Engineering,* vol. 7, pp. 1-14, 2015.

[74] D. D. Luigi, G. Fornetti, M. Guarneri, d. C. Mario Ferri, M. Francucci and M. Nuvoli, “Terrestrial and Subsea 3D Laser Scanners for Cultural Heritage Applications,” *Knowledge, Diagnostics and Preservation of Cultural Heritage,* 2012.

[75] P. X. Huang, B. J. Boom and R. B. Fisher, “Underwater Live Fish Recognition Using a Balance-Guaranteed Optimized Tree,” *Asian Conference on Computer Vision,* pp. 422-433, 2012.

[76] D. J. Lee, R. B. Schoenberger, S. D., X. Xu and P. Zhan, "Contour Matching for Fish Species Recognition and Migration Monitoring," *Two-and Three-Dimensional Vision Systems for Inspection, Control, and Metrology II,* vol. 5606, pp. 37-49, 2004.

[77] S. Corchs, F. Gasparini, F. Marini and R. Schettini, "A sharpness measure on automatically selected edge segments," *Image Quality and System Performance IX,* vol. 8293, 2012.

[78] J. Åhlén, "Colour correction of underwater images using spectral data," *octoral dissertation, Acta Universitatis Upsaliensis,* 2005.

[79] J. S. Jaffe, "Computer modeling and the design of optimal underwater imaging systems," *IEEE Journal of Oceanic Engineering,,* vol. 15, pp. 101-111, 1990.

[80] C. O. Ancuti, C. Ancuti, C. De Vleeschouwer and R. Garcia, "Locally Adaptive Color Correction for Underwater Image Dehazing and Matching.," *Proceedings of the IEEE Conference on Computer Vision and Pattern Recognition Workshops ,* pp. 1-9, 2017.

[81] Y. Y. S. a. N. Karpel., "Clear underwater vision," *Proc. IEEE Computer Society Conference on Computer Vision and Pattern Recognition,* vol. 1, pp. 536-543, 2004.

[82] Y. Y. Schechner and N. Karpel., " Recovery of underwater visibility and structure by polarization analysis," *IEEE Journal of Oceanic Engineering,* vol. 30, pp. 570-587, 2005.

[83] K. Iqbal, R. A. Salam, A. Osman and A. Z. Talib, "Underwater Image Enhancement Using an Integrated Colour Model," *IAENG International Journal of Computer Science,,* vol. 34, 2007.

[84] S. Bazeille, I. Quidu, L. Jaulin and J. P. .. I. (. x. Malkasse, "Automatic underwater image pre-processing," *CMM'06,* 2006.

[85] T. N. R. Garcia and X. Cufi, "On the way to solve lighting problems in underwater imaging," *Proceedings of the IEEE Oceans Conference Record,* vol. 2, pp. 1018-1024, 2002.

[86] M. Borgetto, V. Rigaud and J. F. Lots, "Lighting correction for underwater mosaicking enhancement," *Proceedings of the 16th International Conference on Vision Interface,* 2003.

[87] C. J. Prabhakar and P. U. Kumar, " An image based technique for enhancement of underwater images," *arXiv preprint arXiv,* 2012.

[88] K. Iqbal, R. A. Salam, A. Osman and A. Z. Talib, "Underwater Image Enhancement Using an Integrated Colour Model," *AENG International Journal of Computer Science,* vol. 34, 2007.

[89] K. Iqbal, M. O. Odetayo, A. E. James, R. A. Salam and A. Z. Talib, "Enhancing the low quality images using Unsupervised Colour Correction Method," *SMC ,* pp. 1703-1709, 2010.

[90] A. S. A. Ghani and N. A. M. Isa, "Underwater image quality enhancement through Rayleigh-stretching and averaging image planes," *International Journal of Naval Architecture and Ocean Engineering,* vol. 6, pp. 840-866, 2014.

[91] C. S. Tan, P. Y. Lau, M. C. Lim, J. A. Hi, E. P. Lim, S. M. Phang and T. J. Low, “An Effective Approach for the Underwater Color Image Enhancement.”.

[92] C. Ancuti, C. O. Ancuti, T. Haber and P. Bekaert, “Enhancing underwater images and videos by fusion,” *2012 IEEE Conference on Computer Vision and Pattern Recognition,* pp. 81-88, 2012.

[93] K. Zuiderveld, “Contrast Limited Adaptive Histograph Equalization,” *Graphic Gems IV,* p. 474–485, 1994.

[94] M. Ebner, “The Gray World Assumption, Color constancy,” *John Wiley & Sons.,* vol. 6, 2007.

[95] M. Ebner, “Gamma Correction, Color Constancy,” *John Wiley & Sons,* 2007.

[96] F. Menna, E. Nocerino and F. Remondino, “Flat Versus Hemispherical Dome Ports in Underwater Photogrammetry,” *he International Archives of Photogrammetry, Remote Sensing and Spatial Information Sciences,* pp. 42, 481., 2017.

[97] H. B. K. P., “ Obtaining shape from shading information,” *The Psychology of Computer Vision, McGraw-Hill,* p. 115–155, 1975.

[98] A. P. Pentland, “Local shading analysis,” *Transactions on Pattern Analysis and Machine Intelligence,* p. 170–179, 1984.

[99] B. L., R. F. and S. M., “Automated and accurate orientation of complex image sequences. International Archives of the Photogrammetry,” *Remote Sensing and Spatial Information Sciences ,* pp. 277-284, 2011.

[100] L. D., “Distinctive Image Features from Scale-Invariant Keypoints,” *International Journal of Computer Vision,* vol. 60, pp. 91-110, 2004.

[101] B. H., E. A., T. T. and V. Van Gool L. ., “SURF: Speeded Up Robust Features,” *Computer Vision and Image Understanding,* vol. 110, pp. 346-359, 2008.

[102] F. Remondino, M. G. Spera, E. Nocerino, F. Menna, F. Nex and S. Gonizzi-Barsanti, “Dense image matching: comparisons and analyses,” *Digital Heritage International Congress (DigitalHeritage),* vol. 1, pp. 47-54, 2013.

[103] C. Balletti and F. Guerra, “Image matching for historical maps comparison,” *e-Perimetron,* vol. 4, pp. 180-186, 2009.

[104] M. Vergauwen and L. Van Gool, “Web-based 3D reconstruction service,” *Machine Vision and Application,* vol. 17, pp. 411-426, 2006.

[105] R. S. Berns, “Billmeyer and Saltzman's principles of color technology,” pp. pp. 71-74, 2000.

[106] N. Milić, D. Novaković and N. Kašiković, “Measurement uncertainty in colour characterization of printed textile materials,” *Journal of Graphic Engineering and Design,* vol. 2, 2011.

[107] U. E. Siebeck, N. J. Marshall, A. Klüter and O. Hoegh-Guldberg, “Monitoring coral bleaching using a colour reference card,” *Coral Reefs,* Vols. 25(3),, pp. 453-460, 2006.

[108] D. Litwiller, ““Ccd vs. cmos,”,” *Photonics Spectra,* vol. 35, pp. 154-158, 2001.

[109] P. Meli, “ LA RICOSTRUZIONE 3D IN AMBITO ARCHEOLOGICO E POSSIBILE UTILIZZO NEL CAMPO DELLE INFRASTRUTTURE STRADALI: ANALISI DELLE POTENZIALITA'DELLE TECNICHE IMAGE-BASED.,” 2014.

[110] L. L. C. Agisoft, “Agisoft PhotoScan user manual: professional edition,” 2014.